

A posteriori error analysis of a local adaptive discontinuous Galerkin method for convection-diffusion-reaction equations

Assyr Abdulle *

Giacomo Rosilho de Souza †

May 30, 2022

Abstract

A local adaptive discontinuous Galerkin method for convection-diffusion-reaction equations is introduced. Departing from classical adaptive algorithms, the proposed method is based on a coarse grid and iteratively improves the accuracy of the solution by solving local elliptic problems identified by an a posteriori error control. Based on a flux reconstruction strategy, a posteriori error estimators free of undetermined constants for such a scheme are derived. Numerical comparison with a classical adaptive algorithm illustrate the efficiency and robustness of the new method.

Key words. elliptic equation, local scheme, discontinuous Galerkin, a posteriori error estimators

AMS subject classifications. 65N15, 65N30.

1 Introduction

Solutions to partial differential equations that exhibit singularity (e.g. cracks) or high variations in the computational domain are usually approximated by adaptive numerical methods. There is nowadays a large body of literature concerned with the development of reliable a posteriori error estimators aiming for mesh refinement in regions of large errors (see e.g. [5, 6, 7, 28]). However, classical adaptive methods are usually based on iterative processes which rely on recomputing the solution on the whole computational domain for each new mesh obtained after a refinement procedure.

In this paper we present a scheme which solves local problems defined on refined regions only. Local schemes have been proposed in the past, we mention the Local Defect Correction (LDC) method [18], the Fast Adaptive Composite (FAC) grid algorithm [22] and the Multi-Level Adaptive (MLA) technique [8]. At each iteration, these algorithms solve a problem on a coarse mesh on the whole domain and a local problem on a finer mesh. The coarse solution is used for artificial boundary conditions while the local solution is used to correct the residual in the coarse grid. In [7] the LDC scheme has been coupled with a posteriori error estimators, which are used to select the local domain.

In [1] we proposed a Local Discontinuous Galerkin Gradient Discretization (LDGGD) method which decomposes the computational domain in local subdomains encompassing the large gradient regions. This scheme iteratively improves a coarse solution on the full domain by solving local

*assyр.abdulle@epfl.ch

†giacomo.rosilhodesouza@epfl.ch

École Polytechnique Fédérale de Lausanne (EPFL), SB-MATH-ANMC, Station 8, 1015 Lausanne, Switzerland.

elliptic problems on finer meshes. Hence, the full problem is solved only in the first iteration on a coarse mesh while a sequence of solutions on smaller subdomains are subsequently computed. In turn iterations between subdomains are not needed as in the LDC, FAC or MLA schemes and the condition number of the small systems are considerably smaller than the one of large systems (which describe data and mesh variations on the whole domain). The LDGGD method has been shown to converge under minimal regularity assumptions, i.e. when the solution is in $H_0^1(\Omega)$ and the forcing term in $H^{-1}(\Omega)$ [1]. However, the marking of the subdomains this scheme did so far rely on the a priori knowledge of the location of high gradient regions.

The main contribution of this paper is to propose a posteriori error estimators and derive an a posteriori error analysis for the LDGGD method, which can be used to identify the subdomains to be refined. This is crucial for practical applications of the method. The LDGGD relies on the symmetric weighted interior penalty Galerkin (SWIPG) method [12, 17] and we consider linear advection-diffusion-reaction equations

$$\begin{aligned} -\nabla \cdot (A\nabla u) + \boldsymbol{\beta} \cdot \nabla u + \mu u &= f && \text{in } \Omega, \\ u &= 0 && \text{in } \partial\Omega, \end{aligned}$$

where Ω is an open bounded polytopal connected subset of \mathbb{R}^d for $d \geq 2$, A is the diffusion tensor, $\boldsymbol{\beta}$ the velocity field, μ the reaction coefficient and f a forcing term. In [16] the authors introduce a posteriori error estimators for the SWIPG scheme based on cutoff functions and conforming flux and potential reconstructions, these estimators are shown to be efficient and robust in singularly perturbed regimes. Following the same strategy, we derive estimators for the local scheme by weakening the regularity requirements on the reconstructed fluxes. The new estimators are as well free of unknown constants and their robustness is verified numerically. Furthermore, they are employed to define the local subdomains and provide error bounds on the numerical solution of the LDGGD method.

The outline of the paper is as follows. In Section 2 we describe the local scheme, in Section 3 we introduce the a posteriori error estimators and state the main a posteriori error analysis results. Section 4 is dedicated to the definition of the reconstructed fluxes and proofs of the main results. Finally, various numerical examples illustrating the efficiency and versatility of the proposed method are presented in Section 5.

2 Local adaptive discontinuous Galerkin method

In this section we introduce the local algorithm based on the discontinuous Galerkin method. We start by some assumptions on the data and the domain, before introducing the weak form corresponding to (1.1). We assume that $\Omega \subset \mathbb{R}^d$ is a polytopal domain with $d \geq 2$, $\boldsymbol{\beta} \in W^{1,\infty}(\Omega)^d$, $\mu \in L^\infty(\Omega)$ and $A \in L^\infty(\Omega)^{d \times d}$, with $A(\boldsymbol{x})$ a symmetric piecewise constant matrix with eigenvalues in $[\underline{\lambda}, \bar{\lambda}]$, where $\bar{\lambda} \geq \underline{\lambda} > 0$. Moreover, we assume that $\mu - \frac{1}{2}\nabla \cdot \boldsymbol{\beta} \geq 0$ a.e. in Ω . This term $\mu - \frac{1}{2}\nabla \cdot \boldsymbol{\beta}$ appears in the symmetric part of the operator $\mathcal{B}(\cdot, \cdot)$ defined in (2.2) and hence the assumption $\mu - \frac{1}{2}\nabla \cdot \boldsymbol{\beta} \geq 0$ is needed for coercivity. Finally, we set $f \in L^2(\Omega)$. Under these assumptions, the unique weak solution $u \in H_0^1(\Omega)$ of (1.1) satisfies

$$\mathcal{B}(u, v) = \int_{\Omega} f v \, d\boldsymbol{x} \quad \text{for all } v \in H_0^1(\Omega), \quad (2.1)$$

where

$$\mathcal{B}(u, v) = \int_{\Omega} (A\nabla u \cdot \nabla v + (\boldsymbol{\beta} \cdot \nabla u)v + \mu uv) \, d\boldsymbol{x}. \quad (2.2)$$

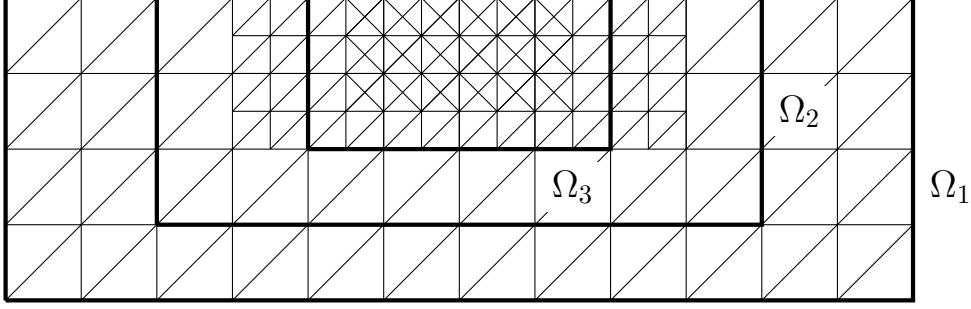


Figure 1. Example of possible meshes for three embedded domains $\Omega_1, \Omega_2, \Omega_3$.

2.1 Preliminary definitions

We start by collecting some notations related to the geometry and the mesh of the subdomains, before recalling the definition of the discontinuous Galerkin finite element method.

Subdomains and meshes

Let $M \in \mathbb{N}$ and $\{\Omega_k\}_{k=1}^M$ be a sequence of open subdomains of Ω with $\Omega_1 = \Omega$. The domains Ω_k for $k \geq 2$ can be any polytopal subset of Ω , in practice they will be chosen by the a posteriori error estimators (see Section 2.2). We consider $\{\mathcal{M}_k\}_{k=1}^M$ a sequence of simplicial meshes on Ω and $\mathcal{F}_k = \mathcal{F}_{k,b} \cup \mathcal{F}_{k,i}$ is the set of boundary and internal faces of \mathcal{M}_k . The assumption below ensures that \mathcal{M}_{k+1} is a refinement of \mathcal{M}_k inside the subdomain Ω_{k+1} .

Assumption 2.1.

1. For each $k = 1, \dots, M$, $\overline{\Omega}_k = \cup_{K \in \mathcal{M}_k, K \subset \Omega_k} \overline{K}$.
2. For $k = 1, \dots, M - 1$,
 - a) $\{K \in \mathcal{M}_{k+1} : K \subset \Omega \setminus \Omega_{k+1}\} = \{K \in \mathcal{M}_k : K \subset \Omega \setminus \Omega_{k+1}\}$,
 - b) if $K, T \in \mathcal{M}_k$ with $K \subset \Omega_{k+1}$, $T \subset \Omega \setminus \Omega_{k+1}$ and $\partial K \cap \partial T \neq \emptyset$ then $K \in \mathcal{M}_{k+1}$,
 - c) if $K \in \mathcal{M}_k$ and $K \subset \Omega_{k+1}$, either $K \in \mathcal{M}_{k+1}$ or K is a union of elements in \mathcal{M}_{k+1} .

Let $\widehat{\mathcal{M}}_k = \{K \in \mathcal{M}_k : K \subset \Omega_k\}$ and $\widehat{\mathcal{F}}_k = \widehat{\mathcal{F}}_{k,b} \cup \widehat{\mathcal{F}}_{k,i}$ the set of faces of $\widehat{\mathcal{M}}_k$, with $\widehat{\mathcal{F}}_{k,b}$ and $\widehat{\mathcal{F}}_{k,i}$ the boundary and internal faces, respectively. Condition 1 in Assumption 2.1 ensures that $\widehat{\mathcal{M}}_k$ is a simplicial mesh on Ω_k . Condition 2 guarantees that in $\Omega \setminus \Omega_{k+1}$ and in the neighborhood of $\partial\Omega_{k+1} \setminus \partial\Omega$ the meshes \mathcal{M}_k and \mathcal{M}_{k+1} are equal and that \mathcal{M}_{k+1} is a refinement of \mathcal{M}_k in Ω_{k+1} . An example of domains and meshes satisfying Assumption 2.1 is illustrated in Figure 1.

Discontinuous Galerkin finite element method

The local adaptive discontinuous Galerkin method will solve local elliptic problems in Ω_k by using a discontinuous Galerkin scheme introduced in [17], which we recall here. In what follows, $\mathfrak{T} = (D, \mathcal{M}, \mathcal{F})$ denotes a tuple defined by a domain D , a simplicial mesh \mathcal{M} on D and its set of faces $\mathcal{F} = \mathcal{F}_b \cup \mathcal{F}_i$. In practice we will consider $\mathfrak{T}_k = (\Omega, \mathcal{M}_k, \mathcal{F}_k)$ or $\widehat{\mathfrak{T}}_k = (\Omega_k, \widehat{\mathcal{M}}_k, \widehat{\mathcal{F}}_k)$. For $\mathfrak{T} = (D, \mathcal{M}, \mathcal{F})$ we define

$$V(\mathfrak{T}) = \{v \in L^2(D) : v|_K \in \mathbb{P}_\ell(K), \forall K \in \mathcal{M}\}, \quad (2.3)$$

where $\mathbb{P}_\ell(K)$ is the set of polynomials in K of total degree ℓ . As usual for such discontinuous Galerkin methods we need to define appropriate averages, jumps, weights and penalization parameters. For $K \in \mathcal{M}$ we denote \mathbf{n}_K the unit normal outward to K and $\mathcal{F}_K = \{\sigma \in \mathcal{F} : \sigma \subset \partial K\}$. Let $\sigma \in \mathcal{F}_i$ and $K, T \in \mathcal{M}$ with $\sigma = \partial K \cap \partial T$, then $\mathbf{n}_\sigma = \mathbf{n}_K$ and

$$\delta_{K,\sigma} = \mathbf{n}_\sigma^\top A|_K \mathbf{n}_\sigma, \quad \delta_{T,\sigma} = \mathbf{n}_\sigma^\top A|_T \mathbf{n}_\sigma.$$

The weights are defined by

$$\omega_{K,\sigma} = \frac{\delta_{T,\sigma}}{\delta_{K,\sigma} + \delta_{T,\sigma}}, \quad \omega_{T,\sigma} = \frac{\delta_{K,\sigma}}{\delta_{K,\sigma} + \delta_{T,\sigma}}$$

and the penalization parameters by

$$\gamma_\sigma = 2 \frac{\delta_{K,\sigma} \delta_{T,\sigma}}{\delta_{K,\sigma} + \delta_{T,\sigma}}, \quad \nu_\sigma = \frac{1}{2} |\boldsymbol{\beta} \cdot \mathbf{n}_\sigma|.$$

If $\sigma \in \mathcal{F}_b$ and $K \in \mathcal{M}$ with $\sigma = \partial K \cap \partial D$ then \mathbf{n}_σ is \mathbf{n}_D the unit outward normal to ∂D and

$$\delta_{K,\sigma} = \mathbf{n}_\sigma^\top A|_K \mathbf{n}_\sigma, \quad \omega_{K,\sigma} = 1, \quad \gamma_\sigma = \delta_{K,\sigma}, \quad \nu_\sigma = \frac{1}{2} |\boldsymbol{\beta} \cdot \mathbf{n}_\sigma|.$$

Let $g \in L^2(\partial D)$, we define the averages and jumps of $v \in V(\mathfrak{T})$ as follows. For $\sigma \in \mathcal{F}_b$ with $\sigma = \partial K \cap \partial D$ we set

$$\{v\}_{\omega,\sigma} = v|_K, \quad \{v\}_{g,\sigma} = \frac{1}{2}(v|_K + g), \quad \llbracket v \rrbracket_{g,\sigma} = v|_K - g$$

and for $\sigma \in \mathcal{F}_i$ with $\sigma = \partial K \cap \partial T$

$$\{v\}_{\omega,\sigma} = \omega_{K,\sigma} v|_K + \omega_{T,\sigma} v|_T, \quad \{v\}_{g,\sigma} = \frac{1}{2}(v|_K + v|_T), \quad \llbracket v \rrbracket_{g,\sigma} = v|_K - v|_T.$$

We define $\llbracket \cdot \rrbracket_\sigma = \llbracket \cdot \rrbracket_{0,\sigma}$ and $\{ \cdot \}_\sigma = \{ \cdot \}_0$. A similar notation holds for vector valued functions and whenever no confusion can arise the subscript σ is omitted. Let h_σ be the diameter of σ and $\eta_\sigma > 0$ a user parameter, for $u, v \in V(\mathfrak{T})$ we define the bilinear form

$$\begin{aligned} \mathcal{B}(u, v, \mathfrak{T}, g) &= \int_D (A \nabla u \cdot \nabla v + (\mu - \nabla \cdot \boldsymbol{\beta}) uv - u \boldsymbol{\beta} \cdot \nabla v) \, dx \\ &\quad - \sum_{\sigma \in \mathcal{F}} \int_\sigma (\llbracket v \rrbracket \{A \nabla u\}_\omega \cdot \mathbf{n}_\sigma + \llbracket u \rrbracket \{A \nabla v\}_\omega \cdot \mathbf{n}_\sigma) \, d\mathbf{y} \\ &\quad + \sum_{\sigma \in \mathcal{F}} \int_\sigma ((\eta_\sigma \frac{\gamma_\sigma}{h_\sigma} + \nu_\sigma) \llbracket u \rrbracket_g \llbracket v \rrbracket + \boldsymbol{\beta} \cdot \mathbf{n}_\sigma \{u\}_g \{v\}_g) \, d\mathbf{y}, \end{aligned} \tag{2.4}$$

where the gradients are taken element wise. The bilinear form $\mathcal{B}(\cdot, \cdot, \mathfrak{T}, g)$ will be used to approximate elliptic problems in D with Dirichlet boundary condition g . This scheme is known as the Symmetric Weighted Interior Penalty (SWIP) scheme [17]. The SWIP method is an improvement of the Interior Penalty scheme (IP) [4], where the weights are defined as $\omega_{K,\sigma} = \omega_{T,\sigma} = 1/2$. The use of diffusivity-dependent averages increases the robustness of the method for problems with strong diffusion discontinuities. The bilinear form defined in (2.4) is mathematically equivalent to other formulations where $v \boldsymbol{\beta} \cdot \nabla u$ or $\nabla \cdot (\boldsymbol{\beta} u) v$ appear instead of $u \boldsymbol{\beta} \cdot \nabla v$ (see [17] and [12, Section 4.6.2]). Our choice of formulation is convenient to express local conservation laws (see [12, Section 2.2.3]).

2.2 Local method algorithm

In this section we present the local scheme. In order to facilitate the comprehension of the method, we start with an informal description and then provide a pseudo-code for the algorithm. We denote u_k the global solutions on Ω and \hat{u}_k the local solutions on Ω_k , which are used to correct the global solutions.

Given a discretization $\mathfrak{T}_1 = (\Omega, \mathcal{M}_1, \mathcal{F}_1)$ on Ω the local scheme computes a first approximate solution $u_1 \in V(\mathfrak{T}_1)$ to (2.1). The algorithm then performs the following steps for $k = 2, \dots, M$.

- i) Given the current solution u_{k-1} , identify the region Ω_k where the error is large and define a new refined mesh \mathcal{M}_k satisfying Assumption 2.1 by iterating the following steps.
 - a) For each element $K \in \mathcal{M}_{k-1}$ compute an error indicator $\eta_{M,K}$ (defined in (3.5)) and mark the local domain Ω_k using the fixed energy fraction marking strategy [13, Section 4.2]. Hence, Ω_k is defined as the union of the elements with largest error indicator $\eta_{M,K}$ and it is such that the error committed inside of Ω_k is at least a prescribed fraction of the total error.
 - b) Define the new mesh \mathcal{M}_k by refining the elements $K \in \mathcal{M}_{k-1}$ with $K \subset \Omega_k$.
 - c) Enlarge the local domain Ω_k defined at step a) by adding a one element wide boundary layer (i.e. in order to satisfy item 2b of Assumption 2.1).
 - d) Define the local mesh $\widehat{\mathcal{M}}_k$ by the elements of \mathcal{M}_k inside of Ω_k .
- ii) Solve a local elliptic problem in Ω_k on the refined mesh $\widehat{\mathcal{M}}_k$ using u_{k-1} as artificial Dirichlet boundary condition on $\partial\Omega_k \setminus \partial\Omega$. The solution is denoted $\hat{u}_k \in V(\widehat{\mathfrak{T}}_k)$, where $\widehat{\mathfrak{T}}_k = (\Omega_k, \widehat{\mathcal{M}}_k, \widehat{\mathcal{F}}_k)$.
- iii) The local solution \hat{u}_k is used to correct the previous solution u_{k-1} inside of Ω_k and obtain the new global solution u_k .

The pseudo-code of the local scheme is given in Algorithm 1, where $\chi_{\Omega \setminus \Omega_k}$ is the indicator function of $\Omega \setminus \Omega_k$ and $(\cdot, \cdot)_k$ is the inner product in $L^2(\Omega_k)$. The function $\text{LocalDomain}(u_k, \mathfrak{T}_k)$ used in Algorithm 1 performs steps a)-d) of i). For purely diffusive problems, it is shown in [26, Theorem 8.2] that Algorithm 1 is equivalent to the LDGGD introduced in [1], hence the scheme convergences for exact solutions $u \in H_0^1(\Omega)$.

Algorithm 1 LocalScheme(\mathfrak{T}_1)

```

Find  $u_1 \in V(\mathfrak{T}_1)$  solution to  $\mathcal{B}(u_1, v_1, \mathfrak{T}_1, 0) = (f, v_1)_1$  for all  $v_1 \in V(\mathfrak{T}_1)$ .
for  $k = 2, \dots, M$  do
     $(\mathfrak{T}_k, \widehat{\mathfrak{T}}_k) = \text{LocalDomain}(u_{k-1}, \mathfrak{T}_{k-1})$ .
     $g_k = u_{k-1} \chi_{\Omega \setminus \Omega_k} \in V(\mathfrak{T}_k)$ .
    Find  $\hat{u}_k \in V(\widehat{\mathfrak{T}}_k)$  solution to  $\mathcal{B}(\hat{u}_k, v_k, \widehat{\mathfrak{T}}_k, g_k) = (f, v_k)_k$  for all  $v_k \in V(\widehat{\mathfrak{T}}_k)$ .
     $u_k = g_k + \hat{u}_k \in V(\mathfrak{T}_k)$ .
end for

```

3 A posteriori error estimators via flux and potential reconstructions

The error estimators used to mark the local domains Ω_k and to provide error bounds on the numerical solution u_k are introduced here.

In the framework of selfadjoint elliptic problems, the equilibrated fluxes method [3, 7] is a technique largely used to derive a posteriori error estimators free of undetermined constants and is based on the definition of local fluxes which satisfy a local conservation property. Since local fluxes and conservation properties are intrinsic to the discontinuous Galerkin formulation, this discretization is well suited for the equilibrated fluxes method [2, 11]. In [14, 20] the Raviart-Thomas-Nédélec space is used to build an $H_{\text{div}}(\Omega)$ conforming reconstruction \mathbf{t}_h of the discrete diffusive flux $-A\nabla u_h$. A diffusive flux \mathbf{t}_h with optimal divergence, in the sense that it coincides with the orthogonal projection of the right-hand side f onto the discontinuous Galerkin space, is obtained. In [16] the authors extend this approach to convection-diffusion-reaction equations by defining an $H_{\text{div}}(\Omega)$ conforming convective flux \mathbf{q}_h approximating βu_h and satisfying a conservation property.

We follow a similar strategy and define in the next section error estimators in function of diffusive and convective fluxes reconstructions $\mathbf{t}_k, \mathbf{q}_k$ for the local scheme, as well as an $H_0^1(\Omega)$ conforming potential reconstruction s_k of the solution u_k .

3.1 A posteriori error estimators

The error estimators in function of the potential reconstruction s_k approximating the solution u_k , the diffusive and convective fluxes \mathbf{t}_k and \mathbf{q}_k approximating $-A\nabla u_k$ and βu_k , respectively, are defined in this section.

Following the iterative and local nature of our scheme, we define the diffusive and convective fluxes reconstructions as

$$\mathbf{t}_k = \mathbf{t}_{k-1}\chi_{\Omega \setminus \Omega_k} + \hat{\mathbf{t}}_k, \quad \mathbf{q}_k = \mathbf{q}_{k-1}\chi_{\Omega \setminus \Omega_k} + \hat{\mathbf{q}}_k, \quad (3.1)$$

where $\mathbf{t}_0 = \mathbf{q}_0 = 0$ and $\hat{\mathbf{t}}_k, \hat{\mathbf{q}}_k$ are $H_{\text{div}}(\Omega_k)$ conforming fluxes reconstructions of $-A\nabla \hat{u}_k, \beta \hat{u}_k$, respectively, and where \hat{u}_k is the local solution. To avoid any abuse of notation in (3.1), we extended $\hat{\mathbf{t}}_k, \hat{\mathbf{q}}_k$ to zero outside of Ω_k . The fluxes reconstructions $\hat{\mathbf{t}}_k, \hat{\mathbf{q}}_k$ satisfy a local conservation property and are defined in Section 4.1. We readily see that (3.1) allows for flux jumps at the subdomains boundaries, while giving enough freedom to define $\hat{\mathbf{t}}_k, \hat{\mathbf{q}}_k$ in a way that a conservation property is satisfied. The fluxes reconstructions are used to measure the non conformity of the numerical fluxes. In the same spirit we define a potential reconstruction $s_k \in H_0^1(\Omega)$ used to measure the non conformity of the numerical solution. It is defined recursively as

$$s_k = s_{k-1}\chi_{\Omega \setminus \Omega_k} + \hat{s}_k, \quad (3.2)$$

where $s_0 = 0$ and $\hat{s}_k \in H^1(\Omega_k)$ is such that $s_k \in H_0^1(\Omega)$; similarly, we extend \hat{s}_k to zero outside of Ω_k . More details about the definitions of $\hat{\mathbf{t}}_k, \hat{\mathbf{q}}_k$ and \hat{s}_k will be given in Section 4.1, for the time being we will define the error estimators.

Let $K \in \mathcal{M}_k, v \in H^1(K)$,

$$\|v\|_K^2 = \|A^{1/2}\nabla v\|_{L^2(K)^d}^2 + \|(\mu - \frac{1}{2}\nabla \cdot \beta)^{1/2}v\|_{L^2(K)}^2, \quad (3.3)$$

where $\|\cdot\|_{L^2(K)}$ is the L^2 -norm for scalar-valued functions in K and $\|\cdot\|_{L^2(K)^d}$ the L^2 -norm for vector-valued functions in K . The non conformity of the numerical solution u_k is measured by the estimator

$$\eta_{NC,K} = \|u_k - s_k\|_K. \quad (3.4a)$$

In the following, $m_K, \tilde{m}_K, m_\sigma, D_{t,K,\sigma}, c_{\beta,\mu,K} > 0$ are some known constants which will be defined in Section 4.2. The residual estimator is

$$\eta_{R,K} = m_K \|f - \nabla \cdot \mathbf{t}_k - \nabla \cdot \mathbf{q}_k - (\mu - \nabla \cdot \boldsymbol{\beta})u_k\|_{L^2(K)}, \quad (3.4b)$$

which can be seen as the residual of (2.1) where we first replace u by u_k , then $-A\nabla u_k$ by \mathbf{t}_k , $\boldsymbol{\beta}u_k$ by \mathbf{q}_k and finally use the Green theorem. The error estimators defined in (3.4c) to (3.4j) measure the error introduced by these substitutions and the error introduced when applying the Green theorem to $\mathbf{t}_k, \mathbf{q}_k$, which are not in $H_{\text{div}}(\Omega)$.

The diffusive flux estimator measures the difference between $-A\nabla u_k$ and \mathbf{t}_k . It is given by $\eta_{DF,K} = \min\{\eta_{DF,K}^1, \eta_{DF,K}^2\}$, where

$$\begin{aligned} \eta_{DF,K}^1 &= \|A^{1/2}\nabla u_k + A^{-1/2}\mathbf{t}_k\|_{L^2(K)^d}, \\ \eta_{DF,K}^2 &= m_K \|(\mathcal{I} - \pi_0)(\nabla \cdot (A\nabla u_k + \mathbf{t}_k))\|_{L^2(K)} \\ &\quad + \tilde{m}_K^{1/2} \sum_{\sigma \in \mathcal{F}_K} C_{t,K,\sigma}^{1/2} \|(A\nabla u_k + \mathbf{t}_k) \cdot \mathbf{n}_\sigma\|_{L^2(\sigma)}, \end{aligned} \quad (3.4c)$$

π_0 is the L^2 -orthogonal projector onto $\mathbb{P}_0(K)$ and \mathcal{I} is the identity operator. Let $\sigma \in \mathcal{F}_k$ and $\pi_{0,\sigma}$ be the L^2 -orthogonal projector onto $\mathbb{P}_0(\sigma)$. The convection and upwinding estimators, that measure the difference between $\boldsymbol{\beta}u_k, \boldsymbol{\beta}s_k$ and \mathbf{q}_k , are defined by

$$\eta_{C,1,K} = m_K \|(\mathcal{I} - \pi_0)(\nabla \cdot (\mathbf{q}_k - \boldsymbol{\beta}s_k))\|_{L^2(K)}, \quad (3.4d)$$

$$\eta_{C,2,K} = \frac{1}{2} c_{\beta,\mu,K}^{-1/2} \|(\nabla \cdot \boldsymbol{\beta})(u_k - s_k)\|_{L^2(K)}, \quad (3.4e)$$

$$\tilde{\eta}_{C,1,K} = m_K \|(\mathcal{I} - \pi_0)(\nabla \cdot (\mathbf{q}_k - \boldsymbol{\beta}u_k))\|_{L^2(K)}, \quad (3.4f)$$

$$\eta_{U,K} = \sum_{\sigma \in \mathcal{F}_K} \chi_\sigma m_\sigma \|\pi_{0,\sigma}\{\{\mathbf{q}_k - \boldsymbol{\beta}s_k\}\} \cdot \mathbf{n}_\sigma\|_{L^2(\sigma)}, \quad (3.4g)$$

$$\tilde{\eta}_{U,K} = \sum_{\sigma \in \mathcal{F}_K} \chi_\sigma m_\sigma \|\pi_{0,\sigma}\{\{\mathbf{q}_k - \boldsymbol{\beta}u_k\}\} \cdot \mathbf{n}_\sigma\|_{L^2(\sigma)}, \quad (3.4h)$$

where $\chi_\sigma = 2$ if $\sigma \in \mathcal{F}_{k,b}$ and $\chi_\sigma = 1$ if $\sigma \in \mathcal{F}_{k,i}$. Finally, we introduce the jump estimators coming from the application of the Green theorem to \mathbf{t}_k and \mathbf{q}_k (see Lemma 4.4). Those are defined by

$$\eta_{\Gamma,1,K} = \frac{1}{2} (|K|c_{\beta,\mu,K})^{-1/2} \sum_{\sigma \in \mathcal{F}_K \cap \mathcal{F}_{k,i}} \|\pi_{0,\sigma}[\mathbf{q}_k] \cdot \mathbf{n}_\sigma\|_{L^1(\sigma)}, \quad (3.4i)$$

$$\eta_{\Gamma,2,K} = \frac{1}{2} \sum_{\sigma \in \mathcal{F}_K \cap \mathcal{F}_{k,i}} D_{t,K,\sigma} \|[\mathbf{t}_k] \cdot \mathbf{n}_\sigma\|_{L^2(\sigma)}. \quad (3.4j)$$

We end the section defining the marking error estimator $\eta_{M,K}$ used to mark Ω_k in the LocalDomain routine of Algorithm 1, let

$$\begin{aligned} \eta_{M,K} &= \eta_{NC,K} + \eta_{R,K} + \alpha \eta_{DF,K} + \eta_{C,1,K} + \eta_{C,2,K} + \alpha \eta_{U,K} \\ &\quad + \eta_{\Gamma,1,K} + \eta_{\Gamma,2,K} + \tilde{\eta}_{C,1,K} + \tilde{\eta}_{U,K}. \end{aligned} \quad (3.5)$$

In practice, the local domains Ω_k , which are defined through $\eta_{M,K}$, can assume any shape and even contain holes. From numerical experiments, we noticed that giving a weight $\alpha > 1$ to the error

estimators $\eta_{DF,K}$ and $\eta_{U,K}$ yields in more regular local domains Ω_k (less holes, smoother boundaries) and thus improves the numerical solutions at a negligible cost. In the numerical experiments of Section 5 we will use $\alpha = 5$.

3.2 Main results

We state here our main results related to the a posteriori analysis of the local scheme, in particular we will provide error bounds on the numerical solution u_k which are free of undetermined constants.

We start defining the norms for which we provide the error bounds, the same norms are used in [16]. The operator \mathcal{B} defined in (2.2) can be written $\mathcal{B} = \mathcal{B}_S + \mathcal{B}_A$, where \mathcal{B}_S and \mathcal{B}_A are symmetric and skew-symmetric operators defined by

$$\begin{aligned}\mathcal{B}_S(u, v) &= \int_{\Omega} (A \nabla u \cdot \nabla v + (\mu - \frac{1}{2} \nabla \cdot \boldsymbol{\beta}) uv) \, d\mathbf{x}, \\ \mathcal{B}_A(u, v) &= \int_{\Omega} (\boldsymbol{\beta} \cdot \nabla u + \frac{1}{2} (\nabla \cdot \boldsymbol{\beta}) u) v \, d\mathbf{x},\end{aligned}$$

for $u, v \in H^1(\mathcal{M}_k)$. The energy norm is defined by the symmetric operator as

$$\|v\|^2 = \mathcal{B}_S(v, v) = \|A^{1/2} \nabla v\|_{L^2(\Omega)^d}^2 + \|(\mu - \frac{1}{2} \nabla \cdot \boldsymbol{\beta})^{1/2} v\|_{L^2(\Omega)}^2,$$

observe that $\|v\|^2 = \sum_{K \in \mathcal{M}_k} \|v\|_K^2$, with $\|\cdot\|_K$ as in (3.3). Since the norm $\|\cdot\|$ is defined by the symmetric operator, it is well suited to study problems with dominant diffusion or reaction. On the other hand, it is inappropriate for convection dominated problems since it lacks a term measuring the error along the velocity direction. For this kind of problems we use the augmented norm

$$\|v\|_{\oplus} = \|v\| + \sup_{\substack{w \in H_0^1(\Omega) \\ \|w\|=1}} (\mathcal{B}_A(v, w) + \mathcal{B}_J(v, w)),$$

where

$$\mathcal{B}_J(v, w) = - \sum_{\sigma \in \mathcal{F}_{k,i}} \int_{\sigma} [\boldsymbol{\beta} v] \cdot \mathbf{n}_{\sigma} \{\{\pi_0 w\}\} \, d\mathbf{y}$$

is a term needed to sharpen the error bounds. The next two theorems give a bound on the error of the local scheme, measured in the energy or the augmented norm.

Theorem 3.1. *Let $u \in H_0^1(\Omega)$ be the solution to (2.1), $u_k \in V(\mathfrak{T}_k)$ given by Algorithm 1, $s_k \in V(\mathfrak{T}_k) \cap H_0^1(\Omega)$ from (3.2) and (4.5) and $\mathbf{t}_k, \mathbf{q}_k \in \mathbf{RTN}_z(\mathcal{M}_k)$ be defined by (3.1) and (4.2). Then, the error measured in the energy norm is bounded as*

$$\|u - u_k\| \leq \eta = \left(\sum_{K \in \mathcal{M}_k} \eta_{NC,K}^2 \right)^{1/2} + \left(\sum_{K \in \mathcal{M}_k} \eta_{1,K}^2 \right)^{1/2},$$

where $\eta_{1,K} = \eta_{R,K} + \eta_{DF,K} + \eta_{C,1,K} + \eta_{C,2,K} + \eta_{U,K} + \eta_{\Gamma,1,K} + \eta_{\Gamma,2,K}$.

Theorem 3.2. *Under the same assumptions of Theorem 3.1, the error measured in the augmented norm is bounded as*

$$\|u - u_k\|_{\oplus} \leq \tilde{\eta} = 2\eta + \left(\sum_{K \in \mathcal{M}_k} \eta_{2,K}^2 \right)^{1/2},$$

with η from Theorem 3.1 and $\eta_{2,K} = \eta_{R,K} + \eta_{DF,K} + \tilde{\eta}_{C,1,K} + \tilde{\eta}_{U,K} + \eta_{\Gamma,1,K} + \eta_{\Gamma,2,K}$.

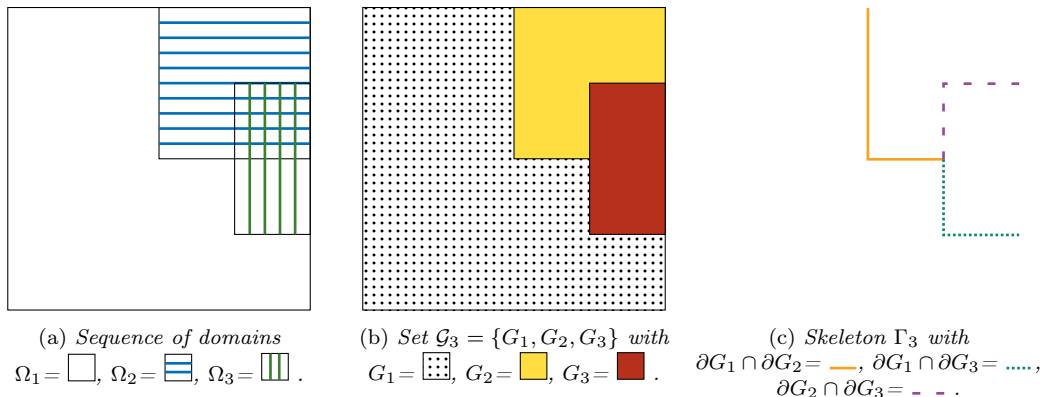


Figure 2. Example of sequence of domains $\Omega_1, \Omega_2, \Omega_3$, set \mathcal{G}_3 and skeleton Γ_3 .

The error estimators of Theorems 3.1 and 3.2 are free of undetermined constants, indeed they depend on the numerical solution, the smallest eigenvalues of the diffusion tensor, on the essential minimum of $\mu - \frac{1}{2} \nabla \cdot \beta$, the mesh size and known geometric constants. In contrast, the error estimators are not efficient, i.e. they cannot be bounded from above by the corresponding norm multiplied by a constant independent from the mesh size. The reason is that, compared to the true errors $\|u - u_k\|$ and $\|u - u_k\|_{\oplus}$, the error estimators $\eta_{\Gamma,1,K}$, $\eta_{\Gamma,2,K}$ have a lower order of convergence. We illustrate this downside numerically in Section 5.1.

4 Potential and fluxes reconstructions, proofs of the main results

In this section, we will define the potential, diffusion and advection reconstructions, define the geometric constants appearing in the error estimators defined in (3.4a) to (3.4j) and finally prove Theorems 3.1 and 3.2.

4.1 Potential and fluxes reconstruction via the equilibrated flux method

We define here the fluxes reconstructions \hat{t}_k , \hat{q}_k of (3.1) and the potential reconstruction \hat{s}_k of (3.2). In what follows we assume that \mathcal{M}_k does not have hanging nodes, i.e. we consider matching meshes, since it simplifies the analysis; however, in practice nonmatching meshes possessing hanging nodes can be employed (as in Section 5). Roughly speaking, the next results are extended to nonmatching meshes by building matching submeshes and computing the error estimators on those submeshes, we refer to [16, Appendix] for the details.

We start defining some broken Sobolev spaces and then the potential and fluxes reconstructions. For $k = 1, \dots, M$ let $\mathcal{G}_k = \{G_j \mid j = 1, \dots, k\}$, where $G_k = \Omega_k$ and

$$G_j = \Omega_j \setminus \cup_{i=j+1}^k \bar{\Omega}_i \quad \text{for } j = 1, \dots, k-1.$$

In Figures 2(a) and 2(b) we give an example of a sequence of domains Ω_k and the corresponding set \mathcal{G}_k . We define the broken spaces

$$\begin{aligned} H_{\text{div}}(\mathcal{G}_k) &= \{\mathbf{v} \in L^2(\Omega)^d : \mathbf{v}|_G \in H_{\text{div}}(G) \text{ for all } G \in \mathcal{G}_k\}, \\ H^1(\mathcal{M}_k) &= \{v \in L^2(\Omega) : v|_K \in H^1(K) \text{ for all } K \in \mathcal{M}_k\}, \end{aligned}$$

the divergence and gradient operators in $H_{\text{div}}(\mathcal{G}_k)$ and $H^1(\mathcal{M}_k)$ are taken element wise. We extend the jump operator $[\![\cdot]\!]_\sigma$ to the broken space $H^1(\mathcal{M}_k)$. We call Γ_k the internal skeleton of \mathcal{G}_k , that is

$$\Gamma_k = \{\partial G_i \cap \partial G_j \mid G_i, G_j \in \mathcal{G}_k, i \neq j\},$$

an example of Γ_k is given in Figure 2(c). For each $\gamma \in \Gamma_k$ we define $\mathcal{F}_\gamma = \{\sigma \in \mathcal{F}_{k,i} \mid \sigma \subset \gamma\}$ and set \mathbf{n}_γ , the normal to γ , as $\mathbf{n}_\gamma|_\sigma = \mathbf{n}_\sigma$. The jump $[\![\cdot]\!]_\gamma$ on γ is defined by $[\![\cdot]\!]_\gamma|_\sigma = [\![\cdot]\!]_\sigma$.

In [16] the reconstructed fluxes live in $H_{\text{div}}(\Omega)$. For the local algorithm we need to build such fluxes using the recursive relation (3.1). This leads to fluxes having jumps across the boundaries of the subdomains, i.e. $\gamma \in \Gamma_k$, hence they lie in the broken space $H_{\text{div}}(\mathcal{G}_k)$. In the rest of this section we explain how to build fluxes which are in an approximation space of $H_{\text{div}}(\mathcal{G}_k)$ and satisfy a local conservation property. We start by introducing a broken version of the usual Raviart-Thomas-Nédélec spaces [23, 25], which we define as

$$\mathbf{RTN}_\varkappa(\mathcal{M}_k) := \{\mathbf{v}_k \in H_{\text{div}}(\mathcal{G}_k) : \mathbf{v}_k|_K \in \mathbf{RTN}_\varkappa(K) \text{ for all } K \in \mathcal{M}_k\}, \quad (4.1)$$

where $\varkappa \in \{\ell - 1, \ell\}$ and $\mathbf{RTN}_\varkappa(K) = \mathbb{P}_\varkappa(K)^d + \mathbf{x}\mathbb{P}_\varkappa(K)$. In order to build functions in $\mathbf{RTN}_\varkappa(\mathcal{M}_k)$ we need a characterization of this space. Let $\mathbf{v}_k \in L^2(\Omega)^d$ such that $\mathbf{v}_k|_K \in \mathbf{RTN}_\varkappa(K)$ for each $K \in \mathcal{M}_k$, it is known that $\mathbf{v}_k \in H_{\text{div}}(\Omega)$ if and only if $[\![\mathbf{v}_k]\!]_\sigma \cdot \mathbf{n}_\sigma = 0$ for all $\sigma \in \mathcal{F}_{k,i}$ (see [12, Lemma 1.24]). Since we search for fluxes \mathbf{v}_k in $H_{\text{div}}(\mathcal{G}_k)$, we relax this condition and allow $[\![\mathbf{v}_k]\!]_\gamma \cdot \mathbf{n}_\gamma \neq 0$ for $\gamma \in \Gamma_k$.

Lemma 4.1. *Let $\mathbf{v}_k \in L^2(\Omega)^d$ be such that $\mathbf{v}_k|_K \in \mathbf{RTN}_\varkappa(K)$ for each $K \in \mathcal{M}_k$, then $\mathbf{v}_k \in \mathbf{RTN}_\varkappa(\mathcal{M}_k)$ if and only if $[\![\mathbf{v}_k]\!]_\sigma \cdot \mathbf{n}_\sigma = 0$ for all $\sigma \notin \cup_{\gamma \in \Gamma_k} \mathcal{F}_\gamma$.*

Proof. Following the lines of [12, Lemma 1.24]. \square

The diffusive and convective fluxes $\mathbf{t}_k, \mathbf{q}_k \in \mathbf{RTN}_\varkappa(\mathcal{M}_k)$ are defined recursively as in (3.1), where $\hat{\mathbf{t}}_k, \hat{\mathbf{q}}_k \in \mathbf{RTN}_\varkappa(\widehat{\mathcal{M}}_k)$, with

$$\mathbf{RTN}_\varkappa(\widehat{\mathcal{M}}_k) := \{\mathbf{v}_k \in H_{\text{div}}(\Omega_k) : \mathbf{v}_k|_K \in \mathbf{RTN}_\varkappa(K) \text{ for all } K \in \widehat{\mathcal{M}}_k\},$$

are given by the relations

$$\begin{aligned} \int_\sigma \hat{\mathbf{t}}_k \cdot \mathbf{n}_\sigma p_k \, d\mathbf{y} &= \int_\sigma (-\{\{A\nabla \hat{u}_k\}\}_\omega \cdot \mathbf{n}_\sigma + \eta_\sigma \frac{\gamma_\sigma}{h_\sigma} [\![\hat{u}_k]\!]_{g_k}) p_k \, d\mathbf{y}, \\ \int_\sigma \hat{\mathbf{q}}_k \cdot \mathbf{n}_\sigma p_k \, d\mathbf{y} &= \int_\sigma (\boldsymbol{\beta} \cdot \mathbf{n}_\sigma \{\{ \hat{u}_k \}\}_{g_k} + \nu_\sigma [\![\hat{u}_k]\!]_{g_k}) p_k \, d\mathbf{y} \end{aligned} \quad (4.2a)$$

for all $\sigma \in \widehat{\mathcal{F}}_k$ and $p_k \in \mathbb{P}_\varkappa(\sigma)$ and

$$\begin{aligned} \int_K \hat{\mathbf{t}}_k \cdot \hat{\mathbf{r}}_k \, d\mathbf{x} &= - \int_K A\nabla \hat{u}_k \cdot \hat{\mathbf{r}}_k \, d\mathbf{x} + \sum_{\sigma \in \mathcal{F}_K} \int_\sigma \omega_{K,\sigma} [\![\hat{u}_k]\!]_{g_k} A|_K \hat{\mathbf{r}}_k \cdot \mathbf{n}_\sigma \, d\mathbf{y}, \\ \int_K \hat{\mathbf{q}}_k \cdot \hat{\mathbf{r}}_k \, d\mathbf{x} &= \int_K \hat{u}_k \boldsymbol{\beta} \cdot \hat{\mathbf{r}}_k \, d\mathbf{x} \end{aligned} \quad (4.2b)$$

for all $K \in \widehat{\mathcal{M}}_k$ and $\hat{\mathbf{r}}_k \in \mathbb{P}_{\varkappa-1}(K)^d$. Since $\hat{\mathbf{t}}_k|_K \cdot \mathbf{n}_\sigma, \hat{\mathbf{q}}_k|_K \cdot \mathbf{n}_\sigma \in \mathbb{P}_\varkappa(\sigma)$ (see [9, Proposition 3.2]) then (4.2a) defines $\hat{\mathbf{t}}_k|_K \cdot \mathbf{n}_\sigma, \hat{\mathbf{q}}_k|_K \cdot \mathbf{n}_\sigma$ on σ . The remaining degrees of freedom are fixed by (4.2b)

[9, Proposition 3.3]. Thanks to (4.2a) we have $[[\hat{\mathbf{t}}_k] \cdot \mathbf{n}_\sigma = 0$ and $[[\hat{\mathbf{q}}_k] \cdot \mathbf{n}_\sigma = 0$ for $\sigma \in \widehat{\mathcal{F}}_{k,i}$ and hence $\hat{\mathbf{t}}_k, \hat{\mathbf{q}}_k \in \mathbf{RTN}_\varkappa(\widehat{\mathcal{M}}_k)$. By construction it follows $\mathbf{t}_k, \mathbf{q}_k \in \mathbf{RTN}_\varkappa(\mathcal{M}_k)$.

Let $K \in \mathcal{M}_k$ and π_\varkappa be the L^2 -orthogonal projector onto $\mathbb{P}_\varkappa(K)$, the following lemma states a local conservation property of the reconstructed fluxes. The proof follows the lines of [16, Lemma 2.1]

Lemma 4.2. *Let $u_k \in V(\mathfrak{T}_k)$ be given by Algorithm 1 and $\mathbf{t}_k, \mathbf{q}_k \in H_{\text{div}}(\mathcal{G}_k)$ defined by (3.1) and (4.2). For all $K \in \mathcal{M}_k$ it holds*

$$(\nabla \cdot \mathbf{t}_k + \nabla \cdot \mathbf{q}_k + \pi_\varkappa((\mu - \nabla \cdot \boldsymbol{\beta})u_k))|_K = \pi_\varkappa f|_K.$$

Proof. Let $K \in \mathcal{M}_k$ and $j = \max\{i = 1, \dots, k : K \subset \Omega_j\}$, then $K \in \widehat{\mathcal{M}}_j$, $\mathbf{t}_k|_K = \hat{\mathbf{t}}_j|_K$, $\mathbf{q}_k|_K = \hat{\mathbf{q}}_j|_K$ and $u_k|_K = \hat{u}_j|_K$. Let $v_j \in \mathbb{P}_\varkappa(K)$, with $v_j = 0$ outside of K , by the Green theorem we have

$$\int_K (\nabla \cdot \hat{\mathbf{t}}_j + \nabla \cdot \hat{\mathbf{q}}_j)v_j \, d\mathbf{x} = - \int_K (\hat{\mathbf{t}}_j + \hat{\mathbf{q}}_j) \cdot \nabla v_j \, d\mathbf{x} + \sum_{\sigma \in \mathcal{F}_K} \int_\sigma v_j (\hat{\mathbf{t}}_j + \hat{\mathbf{q}}_j) \cdot \mathbf{n}_K \, d\mathbf{y} \quad (4.3)$$

and using $\mathcal{B}(\hat{u}_j, v_j, \widehat{\mathfrak{T}}_j, g_j) = (f, v_j)_j$ it follows

$$\begin{aligned} \int_K f v_j \, d\mathbf{x} &= \int_K (A \nabla \hat{u}_j \cdot \nabla v_j + (\mu - \nabla \cdot \boldsymbol{\beta}) \hat{u}_j v_j - \hat{u}_j \boldsymbol{\beta} \cdot \nabla v_j) \, d\mathbf{x} \\ &\quad - \sum_{\sigma \in \mathcal{F}_K} \int_\sigma ([v_j] \{A \nabla \hat{u}_j\}_\omega \cdot \mathbf{n}_\sigma + [\hat{u}_j]_{g_j} \{A \nabla v_j\}_\omega \cdot \mathbf{n}_\sigma) \, d\mathbf{y} \\ &\quad + \sum_{\sigma \in \mathcal{F}_K} \int_\sigma ((\eta_\sigma \frac{\gamma_\sigma}{h_\sigma} + \nu_\sigma) [\hat{u}_j]_{g_j} [v_j] + \boldsymbol{\beta} \cdot \mathbf{n}_\sigma \{ \hat{u}_j \}_{g_j} [v_j]) \, d\mathbf{y}. \end{aligned}$$

Since $\{A \nabla v_j\}_\omega = \omega_{K,\sigma} A|_K \nabla v_j$ and $[v_j] \mathbf{n}_\sigma = v_j|_K \mathbf{n}_K$, using (4.2) and (4.3), we obtain

$$\int_K f v_j \, d\mathbf{x} = \int_K (\nabla \cdot \hat{\mathbf{t}}_j + \nabla \cdot \hat{\mathbf{q}}_j + (\mu - \nabla \cdot \boldsymbol{\beta}) \hat{u}_j) v_j \, d\mathbf{x} \quad (4.4)$$

and the result follows from $\nabla \cdot \hat{\mathbf{t}}_j, \nabla \cdot \hat{\mathbf{q}}_j \in \mathbb{P}_\varkappa(K)$, $\mathbf{t}_k|_K = \hat{\mathbf{t}}_j|_K$, $\mathbf{q}_k|_K = \hat{\mathbf{q}}_j|_K$ and $u_k|_K = \hat{u}_j|_K$. \square

In order to define the $H_0^1(\Omega)$ conforming approximation s_k of u_k we will need the so-called Oswald operator already considered in [19] for a posteriori estimates. Let $\mathfrak{T} = (D, \mathcal{M}, \mathcal{F})$, $g \in C^0(\partial D)$ and consider $\mathcal{O}_{\mathfrak{T},g} : V(\mathfrak{T}) \rightarrow V(\mathfrak{T}) \cap H^1(D)$, for a function $v \in V(\mathfrak{T})$ the value of $\mathcal{O}_{\mathfrak{T},g}v$ is prescribed at the Lagrange interpolation nodes p of the conforming finite element space $V(\mathfrak{T}) \cap H^1(D)$. Let $p \in \overline{D}$ be a Lagrange node, if $p \notin \partial D$ we set

$$\mathcal{O}_{\mathfrak{T},g}v(p) = \frac{1}{\#\mathcal{M}_p} \sum_{K \in \mathcal{M}_p} v|_K(p),$$

where $\mathcal{M}_p = \{K \in \mathcal{M} : p \in \overline{K}\}$. If instead $p \in \partial D$ then $\mathcal{O}_{\mathfrak{T},g}v(p) = g(p)$, where g is the Dirichlet condition on ∂D . The reconstructed potential $s_k \in V(\mathfrak{T}_k) \cap H_0^1(\Omega)$ is built as in (3.2), where

$$\hat{s}_k = \mathcal{O}_{\widehat{\mathfrak{T}}_k, s_{k-1}} \hat{u}_k. \quad (4.5)$$

4.2 Constants definition and preliminary results

Here we define the constants appearing in (3.4a) to (3.4j) and derive preliminary results needed to prove Theorems 3.1 and 3.2.

Let $K \in \mathcal{M}_k$ and $\sigma \in \mathcal{F}_K$, we recall that $|K|$ is the measure of K and $|\sigma|$ the $d-1$ dimensional measure of σ . We denote by $c_{A,K}$ the minimal eigenvalue of $A|_K$. Next, we denote by $c_{\beta,\mu,K}$ the essential minimum of $\mu - \frac{1}{2}\nabla \cdot \beta \geq 0$ on K . In what follows we will assume that $\mu - \frac{1}{2}\nabla \cdot \beta > 0$ a.e. in Ω , hence $c_{\beta,\mu,K} > 0$ for all $K \in \mathcal{M}_k$, and provide error estimators under this assumption. We explain in Section 4.4 how to overcome this limitation slightly modifying the proofs and error estimators.

The cutoff functions m_K, \tilde{m}_K and m_σ are defined by

$$\begin{aligned} m_K &= \min\{C_p^{1/2}h_K c_{A,K}^{-1/2}, c_{\beta,\mu,K}^{-1/2}\}, \\ \tilde{m}_K &= \min\{(C_p + C_p^{1/2})h_K c_{A,K}^{-1}, h_K^{-1}c_{\beta,\mu,K}^{-1} + c_{\beta,\mu,K}^{-1/2}c_{A,K}^{-1/2}/2\}, \\ m_\sigma^2 &= \min\{\max_{K \in \mathcal{M}_\sigma} \{3d|\sigma|h_K^2|K|^{-1}c_{A,K}^{-1}\}, \max_{K \in \mathcal{M}_\sigma} \{|\sigma||K|^{-1}c_{\beta,\mu,K}^{-1}\}\}, \end{aligned}$$

where $C_p = 1/\pi^2$ is an optimal Poincaré constant for convex domains [24]. Let $v \in H^1(\mathcal{M}_k)$, it holds

$$\|v - \pi_0 v\|_{L^2(K)} \leq m_K \|v\|_K \quad \text{for all } K \in \mathcal{M}_k, \quad (4.7a)$$

$$\|v - \pi_0 v|_K\|_{L^2(\sigma)} \leq C_{t,K,\sigma}^{1/2} \tilde{m}_K^{1/2} \|v\|_K \quad \text{for all } \sigma \in \mathcal{F}_k \text{ and } K \in \mathcal{M}_\sigma, \quad (4.7b)$$

$$\|[\pi_0 v]\|_{L^2(\sigma)} \leq m_\sigma \sum_{K \in \mathcal{M}_\sigma} \|v\|_K \quad \text{for all } \sigma \in \mathcal{F}_k, \quad (4.7c)$$

where $\mathcal{M}_\sigma = \{K \in \mathcal{M}_k : \sigma \subset \partial K\}$ and $C_{t,K,\sigma}$ is the constant of the trace inequality

$$\|v|_K\|_{L^2(\sigma)}^2 \leq C_{t,K,\sigma} (h_K^{-1} \|v\|_{L^2(K)}^2 + \|v\|_{L^2(K)} \|\nabla v\|_{L^2(K)^d}). \quad (4.8)$$

It has been proved in [27, Lemma 3.12] that for a simplex it holds $C_{t,K,\sigma} = |\sigma|h_K/|K|$.

Let us briefly explain the role of constants (4.6) and how the bounds (4.7) are obtained. We observe that for each bound in (4.7) the cut off functions take the minimum between two possible values, allowing for robust error estimation in singularly perturbed regimes. For (4.7a), using the Poincaré inequality [24, equation 3.2] we have

$$\begin{aligned} \|v - \pi_0 v\|_{L^2(K)} &\leq C_p^{1/2} h_K \|\nabla v\|_{L^2(K)^d} \\ &\leq C_p^{1/2} h_K c_{A,K}^{-1/2} \|A^{1/2} \nabla v\|_{L^2(K)^d} \leq C_p^{1/2} h_K c_{A,K}^{-1/2} \|v\|_K. \end{aligned} \quad (4.9a)$$

Denoting $(\cdot, \cdot)_K$ the $L^2(K)$ inner product, it holds

$$\|v - \pi_0 v\|_{L^2(K)}^2 = (v - \pi_0 v, v - \pi_0 v)_K = (v - \pi_0 v, v)_K \leq \|v - \pi_0 v\|_{L^2(K)} \|v\|_{L^2(K)},$$

hence

$$\|v - \pi_0 v\|_{L^2(K)} \leq \|v\|_{L^2(K)} \leq c_{\beta,\mu,K}^{-1/2} \left(\mu - \frac{1}{2}\nabla \cdot \beta\right)^{1/2} \|v\|_{L^2(K)} \leq c_{\beta,\mu,K}^{-1/2} \|v\|_K \quad (4.9b)$$

and (4.7a) follows. The choice between bounds (4.9a) and (4.9b) depends on whether the problem is singularly perturbed or not. Bounds (4.7b) and (4.7c) are obtained similarly, see [10, Lemma 4.2]

and [29, Lemma 4.5]. Finally, for $K \in \mathcal{M}_k$ and $\sigma \in \mathcal{F}_K$ we define

$$D_{t,K,\sigma} = \left(\frac{C_{t,K,\sigma}}{2h_K c_{\beta,\mu,K}} \left(1 + \sqrt{1 + h_K^2 \frac{c_{\beta,\mu,K}}{c_{A,K}}} \right) \right)^{1/2}, \quad (4.10)$$

which is used to bound $\|v|_K\|_{L^2(\sigma)}$ in terms of $\|v\|_K$ in the next lemma.

Lemma 4.3. *Let $v_k \in H^1(\mathcal{M}_k)$, for each $K \in \mathcal{M}_k$ and $\sigma \in \mathcal{F}_K$ it holds*

$$\|v_k|_K\|_{L^2(\sigma)} \leq D_{t,K,\sigma} \|v_k\|_K.$$

Proof. Let $v_k \in H^1(\mathcal{M}_k)$ and $\epsilon > 0$. Applying Hölder inequality to the trace inequality (4.8) we get

$$\|v_k|_K\|_{L^2(\sigma)}^2 \leq C_{t,K,\sigma} \left((h_K^{-1} + \frac{1}{2\epsilon}) \|v_k\|_{L^2(K)}^2 + \frac{\epsilon}{2} \|\nabla v_k\|_{L^2(K)^d}^2 \right).$$

Hence, if there exists $D_{t,K,\sigma} > 0$ independent of v_k such that

$$\begin{aligned} C_{t,K,\sigma} \left((h_K^{-1} + \frac{1}{2\epsilon}) \|v_k\|_{L^2(K)}^2 + \frac{\epsilon}{2} \|\nabla v_k\|_{L^2(K)^d}^2 \right) \\ \leq D_{t,K,\sigma}^2 (c_{A,K} \|\nabla v_k\|_{L^2(K)^d}^2 + c_{\beta,\mu,K} \|v_k\|_{L^2(K)}^2) \end{aligned} \quad (4.11)$$

then $\|v_k|_K\|_{L^2(\sigma)}^2 \leq D_{t,K,\sigma}^2 \|v_k\|_K^2$ and the result holds. Relation (4.11) holds if

$$C_{t,K,\sigma} (h_K^{-1} + \frac{1}{2\epsilon}) \leq D_{t,K,\sigma}^2 c_{\beta,\mu,K}, \quad C_{t,K,\sigma} \frac{\epsilon}{2} \leq D_{t,K,\sigma}^2 c_{A,K}$$

and hence $D_{t,K,\sigma}^2 = \max\{C_{t,K,\sigma} (h_K^{-1} + \frac{1}{2\epsilon}) c_{\beta,\mu,K}^{-1}, C_{t,K,\sigma} \frac{\epsilon}{2} c_{A,K}^{-1}\}$. Taking ϵ such that the maximum is minimized we get $D_{t,K,\sigma}$ as in (4.10). \square

The proof of the following Lemma is inspired from [16, Theorem 3.1], the main difference is that we take into account the weaker regularity of the reconstructed fluxes.

Lemma 4.4. *Let $u \in H_0^1(\Omega)$ be the solution to (2.1), $u_k \in V(\mathfrak{T}_k)$ given by Algorithm 1, $s_k \in H_0^1(\Omega)$ from (3.2) and (4.5), $\mathbf{t}_k, \mathbf{q}_k \in H_{\text{div}}(\mathcal{G}_k)$ defined by (3.1) and (4.2) and $v \in H_0^1(\Omega)$. Then*

$$|\mathcal{B}(u - u_k, v) + \mathcal{B}_A(u_k - s_k, v)| \leq \left(\sum_{K \in \mathcal{M}_k} \eta_{1,K}^2 \right)^{1/2} \|v\|,$$

with $\eta_{1,K} = \eta_{R,K} + \eta_{DF,K} + \eta_{C,1,K} + \eta_{C,2,K} + \eta_{U,K} + \eta_{\Gamma,1,K} + \eta_{\Gamma,2,K}$.

Proof. Since u satisfies (2.1), using the definition of \mathcal{B} and \mathcal{B}_A

$$\begin{aligned} \mathcal{B}(u - u_k, v) + \mathcal{B}_A(u_k - s_k, v) &= \int_{\Omega} (f - (\mu - \nabla \cdot \beta) u_k) v \, d\mathbf{x} - \int_{\Omega} A \nabla u_k \cdot \nabla v \, d\mathbf{x} \\ &\quad - \int_{\Omega} \frac{1}{2} (\nabla \cdot \beta) (u_k - s_k) v \, d\mathbf{x} - \int_{\Omega} \nabla \cdot (\beta s_k) v \, d\mathbf{x}. \end{aligned}$$

Using $v\mathbf{t}_k \in H_{\text{div}}(\mathcal{G}_k)$, from the divergence theorem we have

$$\begin{aligned} \int_{\Omega} (v\nabla \cdot \mathbf{t}_k + \nabla v \cdot \mathbf{t}_k) \, d\mathbf{x} &= \sum_{G \in \mathcal{G}_k} \int_G \nabla \cdot (v\mathbf{t}_k) \, d\mathbf{x} = \sum_{G \in \mathcal{G}_k} \int_{\partial G} v\mathbf{t}_k \cdot \mathbf{n}_{\partial G} \, d\mathbf{y} \\ &= \sum_{\gamma \in \Gamma_k} \int_{\gamma} \llbracket v\mathbf{t}_k \rrbracket \cdot \mathbf{n}_{\gamma} \, d\mathbf{y} = \sum_{\gamma \in \Gamma_k} \int_{\gamma} \llbracket \mathbf{t}_k \rrbracket \cdot \mathbf{n}_{\gamma} v \, d\mathbf{y} \end{aligned}$$

and hence

$$\begin{aligned} \mathcal{B}(u - u_k, v) + \mathcal{B}_A(u_k - s_k, v) &= \int_{\Omega} (f - \nabla \cdot \mathbf{t}_k - \nabla \cdot \mathbf{q}_k - (\mu - \nabla \cdot \boldsymbol{\beta})u_k)v \, d\mathbf{x} \\ &\quad - \int_{\Omega} \frac{1}{2}(\nabla \cdot \boldsymbol{\beta})(u_k - s_k)v \, d\mathbf{x} + \int_{\Omega} \nabla \cdot (\mathbf{q}_k - \boldsymbol{\beta}s_k)v \, d\mathbf{x} \\ &\quad - \int_{\Omega} (A\nabla u_k + \mathbf{t}_k) \cdot \nabla v \, d\mathbf{x} + \sum_{\gamma \in \Gamma_k} \int_{\gamma} \llbracket \mathbf{t}_k \rrbracket \cdot \mathbf{n}_{\gamma} v \, d\mathbf{y}. \end{aligned} \quad (4.12)$$

From Lemma 4.2 we deduce

$$\begin{aligned} &\left| \int_{\Omega} (f - \nabla \cdot \mathbf{t}_k - \nabla \cdot \mathbf{q}_k - (\mu - \nabla \cdot \boldsymbol{\beta})u_k)v \, d\mathbf{x} \right| \\ &= \left| \int_{\Omega} (f - \nabla \cdot \mathbf{t}_k - \nabla \cdot \mathbf{q}_k - (\mu - \nabla \cdot \boldsymbol{\beta})u_k)(v - \pi_0 v) \, d\mathbf{x} \right| \\ &\leq \sum_{K \in \mathcal{M}_k} \eta_{R,K} \|v\|_K. \end{aligned} \quad (4.13a)$$

Similarly, we get

$$\begin{aligned} \left| \int_{\Omega} (A\nabla u_k + \mathbf{t}_k) \cdot \nabla v \, d\mathbf{x} \right| &\leq \sum_{K \in \mathcal{M}_k} \eta_{DF,K} \|v\|_K, \\ \left| \int_{\Omega} \frac{1}{2}(\nabla \cdot \boldsymbol{\beta})(u_k - s_k)v \, d\mathbf{x} \right| &\leq \sum_{K \in \mathcal{M}_k} \eta_{C,2,K} \|v\|_K. \end{aligned} \quad (4.13b)$$

Since $\llbracket \mathbf{t}_k \rrbracket_{\sigma} = 0$ for $\sigma \in \mathcal{F}_{k,i} \setminus \cup_{\gamma \in \Gamma_k} \mathcal{F}_{\gamma}$, it holds

$$\sum_{\gamma \in \Gamma_k} \int_{\gamma} \llbracket \mathbf{t}_k \rrbracket \cdot \mathbf{n}_{\gamma} v \, d\mathbf{y} = \sum_{\sigma \in \mathcal{F}_{k,i}} \int_{\sigma} \llbracket \mathbf{t}_k \rrbracket \cdot \mathbf{n}_{\sigma} v \, d\mathbf{y} = \frac{1}{2} \sum_{K \in \mathcal{M}_k} \sum_{\sigma \in \mathcal{F}_K \cap \mathcal{F}_{k,i}} \int_{\sigma} \llbracket \mathbf{t}_k \rrbracket \cdot \mathbf{n}_{\sigma} v \, d\mathbf{y}.$$

Using Lemma 4.3 we obtain

$$\begin{aligned} \left| \sum_{\gamma \in \Gamma_k} \int_{\gamma} \llbracket \mathbf{t}_k \rrbracket \cdot \mathbf{n}_{\gamma} v \, d\mathbf{y} \right| &\leq \frac{1}{2} \sum_{K \in \mathcal{M}_k} \sum_{\sigma \in \mathcal{F}_K \cap \mathcal{F}_{k,i}} \|\llbracket \mathbf{t}_k \rrbracket \cdot \mathbf{n}_{\sigma}\|_{L^2(\sigma)} \|v\|_{L^2(\sigma)} \\ &\leq \sum_{K \in \mathcal{M}_k} \eta_{\Gamma,2,K} \|v\|_K. \end{aligned} \quad (4.13c)$$

It remains to estimate $\int_{\Omega} \nabla \cdot (\mathbf{q}_k - \boldsymbol{\beta}s_k)v \, d\mathbf{x}$. For that, we use

$$\begin{aligned} \int_{\Omega} \nabla \cdot (\mathbf{q}_k - \boldsymbol{\beta}s_k)v \, d\mathbf{x} &= \sum_{K \in \mathcal{M}_k} \int_K (\mathcal{I} - \pi_0) \nabla \cdot (\mathbf{q}_k - \boldsymbol{\beta}s_k)(v - \pi_0 v) \, d\mathbf{x} \\ &\quad + \sum_{K \in \mathcal{M}_k} \sum_{\sigma \in \mathcal{F}_K} \int_{\sigma} (\mathbf{q}_k - \boldsymbol{\beta}s_k) \cdot \mathbf{n}_K \pi_0 v \, d\mathbf{y} \end{aligned}$$

and from (4.7a) we get

$$\left| \sum_{K \in \mathcal{M}_k} \int_K (\mathcal{I} - \pi_0) \nabla \cdot (\mathbf{q}_k - \boldsymbol{\beta} s_k) (v - \pi_0 v) \, d\mathbf{x} \right| \leq \sum_{K \in \mathcal{M}_k} \eta_{C,1,K} \|v\|_K. \quad (4.13d)$$

For the second term we write

$$\begin{aligned} & \sum_{K \in \mathcal{M}_k} \sum_{\sigma \in \mathcal{F}_K} \int_{\sigma} (\mathbf{q}_k - \boldsymbol{\beta} s_k) \cdot \mathbf{n}_K \pi_0 v \, d\mathbf{y} = \sum_{\sigma \in \mathcal{F}_k} \int_{\sigma} \llbracket \pi_{0,\sigma} (\mathbf{q}_k - \boldsymbol{\beta} s_k) \pi_0 v \rrbracket \cdot \mathbf{n}_{\sigma} \, d\mathbf{y} \\ & = \sum_{\sigma \in \mathcal{F}_{k,i}} \int_{\sigma} \{\pi_0 v\} \llbracket \pi_{0,\sigma} (\mathbf{q}_k - \boldsymbol{\beta} s_k) \rrbracket \cdot \mathbf{n}_{\sigma} + \llbracket \pi_0 v \rrbracket \{\pi_{0,\sigma} (\mathbf{q}_k - \boldsymbol{\beta} s_k)\} \cdot \mathbf{n}_{\sigma} \, d\mathbf{y} \\ & \quad + \sum_{\sigma \in \mathcal{F}_{k,b}} \int_{\sigma} \pi_0 v \pi_{0,\sigma} (\mathbf{q}_k - \boldsymbol{\beta} s_k) \cdot \mathbf{n}_{\sigma} \, d\mathbf{y} = \text{I} + \text{II} + \text{III} \end{aligned}$$

and we easily obtain, since $\llbracket \boldsymbol{\beta} s_k \rrbracket = 0$,

$$\text{I} = \frac{1}{2} \sum_{K \in \mathcal{M}_k} \sum_{\sigma \in \mathcal{F}_K \cap \mathcal{F}_{k,i}} \int_{\sigma} \pi_0 v|_K \llbracket \pi_{0,\sigma} \mathbf{q}_k \rrbracket \cdot \mathbf{n}_{\sigma} \, d\mathbf{y}.$$

Using $|\pi_0 v|_K| = |K|^{-1/2} \|\pi_0 v\|_{L^2(K)} \leq |K|^{-1/2} \|v\|_{L^2(K)} \leq (|K| c_{\boldsymbol{\beta},\mu,K})^{-1/2} \|v\|_K$ we get

$$\text{I} \leq \frac{1}{2} \sum_{K \in \mathcal{M}_k} \sum_{\sigma \in \mathcal{F}_K \cap \mathcal{F}_{k,i}} (|K| c_{\boldsymbol{\beta},\mu,K})^{-1/2} \|\llbracket \pi_{0,\sigma} \mathbf{q}_k \rrbracket \cdot \mathbf{n}_{\sigma}\|_{L^1(\sigma)} \|v\|_K = \sum_{K \in \mathcal{M}_k} \eta_{\Gamma,1,K} \|v\|_K. \quad (4.13e)$$

Let $\mathcal{M}_{\sigma} = \{K \in \mathcal{M}_k : \sigma \subset \partial K\}$, using (4.7c) for the second term we have

$$\begin{aligned} \text{II} & \leq \sum_{\sigma \in \mathcal{F}_{k,i}} m_{\sigma} \|\pi_{0,\sigma} \{\mathbf{q}_k - \boldsymbol{\beta} s_k\} \cdot \mathbf{n}_{\sigma}\|_{L^2(\sigma)} \sum_{K \in \mathcal{M}_{\sigma}} \|v\|_K \\ & = \sum_{K \in \mathcal{M}_k} \sum_{\sigma \in \mathcal{F}_K \cap \mathcal{F}_{k,i}} m_{\sigma} \|\pi_{0,\sigma} \{\mathbf{q}_k - \boldsymbol{\beta} s_k\} \cdot \mathbf{n}_{\sigma}\|_{L^2(\sigma)} \|v\|_K. \end{aligned}$$

For the last term we similarly obtain

$$\text{III} \leq \sum_{K \in \mathcal{M}_k} \sum_{\sigma \in \mathcal{F}_K \cap \mathcal{F}_{k,b}} m_{\sigma} \|\pi_{0,\sigma} (\mathbf{q}_k - \boldsymbol{\beta} s_k) \cdot \mathbf{n}_{\sigma}\|_{L^2(\sigma)} \|v\|_K$$

and hence

$$\text{II} + \text{III} \leq \sum_{K \in \mathcal{M}_k} \sum_{\sigma \in \mathcal{F}_K} \chi_{\sigma} m_{\sigma} \|\pi_{0,\sigma} \{\mathbf{q}_k - \boldsymbol{\beta} s_k\} \cdot \mathbf{n}_{\sigma}\|_{L^2(\sigma)} \|v\|_K = \sum_{K \in \mathcal{M}_k} \eta_{U,K} \|v\|_K, \quad (4.13f)$$

where $\chi_{\sigma} = 2$ if $\sigma \in \mathcal{F}_{k,b}$ and $\chi_{\sigma} = 1$ if $\sigma \in \mathcal{F}_{k,i}$. Plugging relations (4.13a) to (4.13f) into (4.12) we get the result. \square

In Lemma 4.4 we use Lemma 4.2 to deduce that

$$\int_K (\nabla \cdot \mathbf{t}_k + \nabla \cdot \mathbf{q}_k + (\mu - \nabla \cdot \boldsymbol{\beta}) u_k) \, d\mathbf{x} = \int_K f \, d\mathbf{x} \quad (4.14)$$

and hence (4.13a). However, when the mesh has hanging nodes inside of the local domains Lemma 4.2 is not valid. Indeed, if $\widehat{\mathcal{M}}_k$ has hanging nodes, the fluxes $\hat{\mathbf{t}}_k, \hat{\mathbf{q}}_k$ must be constructed on a matching (free of hanging nodes) submesh $\overline{\mathcal{M}}_k$ of $\widehat{\mathcal{M}}_k$, otherwise they may fail to be in $H_{\text{div}}(\Omega_k)$. The constructed fluxes will satisfy relation (4.4), but since $\nabla \cdot \hat{\mathbf{t}}_k, \nabla \cdot \hat{\mathbf{q}}_k \in \mathbb{P}_2(K')$ for $K' \in \overline{\mathcal{M}}_k$ and $\overline{\mathcal{M}}_k$ is finer than $\widehat{\mathcal{M}}_k$, then we cannot conclude as we did in Lemma 4.2. Nonetheless, (4.4) still implies (4.14), which is enough to prove Lemma 4.4.

4.3 Proof of the theorems

Here we prove Theorems 3.1 and 3.2. We will consider $\mathcal{B} : H_0^1(\Omega) \times H_0^1(\Omega) \rightarrow \mathbb{R}$ defined in (2.2) for functions in $H^1(\mathcal{M}_k)$.

Proof of Theorem 3.1. It has been proved in [15, Lemma 3.1] that for any $u_k \in V(\mathfrak{T}_k)$ and $u, s \in H_0^1(\Omega)$ it holds

$$\|u - u_k\| \leq \|u_k - s\| + |\mathcal{B}(u - u_k, v) + \mathcal{B}_A(u_k - s, v)|,$$

with $v = (u - s)/\|u - s\|$. Choosing u as the exact solution to (2.1), u_k given by Algorithm 1, $s = s_k$ from (3.2) and using Lemma 4.4 gives the result. \square

Proof of Theorem 3.2. Since $u \in H_0^1(\Omega)$ it holds $\mathcal{B}_J(u, w) = 0$ for all $w \in H_0^1(\Omega)$, using $\mathcal{B}_A \leq \mathcal{B} + |\mathcal{B}_S|$ we get

$$\|u - u_k\|_{\oplus} \leq 2\|u - u_k\| + \sup_{\substack{w \in H_0^1(\Omega) \\ \|w\|=1}} (\mathcal{B}(u - u_k, w) - \mathcal{B}_J(u_k, w)).$$

To conclude the proof we show that

$$\sup_{\substack{w \in H_0^1(\Omega) \\ \|w\|=1}} (\mathcal{B}(u - u_k, w) - \mathcal{B}_J(u_k, w)) \leq \left(\sum_{K \in \mathcal{M}_k} \eta_{2,K}^2 \right)^{1/2}.$$

Following Lemma 4.4, we easily get

$$\begin{aligned} \mathcal{B}(u - u_k, w) - \mathcal{B}_J(u_k, w) &\leq \sum_{K \in \mathcal{M}_k} (\eta_{R,K} + \eta_{DF,K} + \tilde{\eta}_{C,1,K} + \eta_{\Gamma,2,K}) \|w\|_K \\ &\quad + \sum_{K \in \mathcal{M}_k} \sum_{\sigma \in \mathcal{F}_K} \int_{\sigma} \pi_0 w (\mathbf{q}_k - \beta u_k) \cdot \mathbf{n}_K \, d\mathbf{y} - \mathcal{B}_J(u_k, w). \end{aligned}$$

The two last terms satisfy

$$\begin{aligned} &\sum_{\sigma \in \mathcal{F}_k} \int_{\sigma} \llbracket \pi_0 w (\mathbf{q}_k - \beta u_k) \rrbracket \cdot \mathbf{n}_{\sigma} \, d\mathbf{y} - \mathcal{B}_J(u_k, w) \\ &= \sum_{\sigma \in \mathcal{F}_k} \chi_{\sigma} \int_{\sigma} \llbracket \pi_0 w \rrbracket \pi_{0,\sigma} \{ \mathbf{q}_k - \beta u_k \} \cdot \mathbf{n}_{\sigma} \, d\mathbf{y} + \sum_{\sigma \in \mathcal{F}_{k,i}} \int_{\sigma} \{ \pi_0 w \} \llbracket \pi_{0,\sigma} \mathbf{q}_k \rrbracket \cdot \mathbf{n}_{\sigma} \, d\mathbf{y} \\ &\leq \sum_{K \in \mathcal{M}_k} (\tilde{\eta}_{U,K} + \eta_{\Gamma,1,K}) \|w\|_K, \end{aligned}$$

where in the last step we followed again Lemma 4.4. \square

4.4 Alternative error bounds

Our aim here is to explain how to avoid the assumption $c_{\beta,\mu,K} > 0$ for all $K \in \mathcal{M}_k$ made in Sections 3.1 and 4.2. This assumption is needed to define $\eta_{\Gamma,1,K}$, $\eta_{\Gamma,2,K}$ but can be avoided if (4.13c) and (4.13e) are estimated differently. For (4.13c), using the trace inequality (4.8) we get

$$\begin{aligned} \left| \sum_{\gamma \in \Gamma_k} \int_{\gamma} \llbracket \mathbf{t}_k \rrbracket \cdot \mathbf{n}_{\gamma} v \, d\mathbf{y} \right| &\leq \frac{1}{2} \sum_{K \in \mathcal{M}_k} \sum_{\sigma \in \mathcal{F}_K \cap \mathcal{F}_{k,i}} \|\llbracket \mathbf{t}_k \rrbracket \cdot \mathbf{n}_{\sigma}\|_{L^2(\sigma)} \|v|_K\|_{L^2(\sigma)} \\ &\leq \sum_{K \in \mathcal{M}_k} \tilde{\eta}_{\Gamma,2,K} (\|v\|_{L^2(K)}^2 + h_K \|v\|_{L^2(K)} \|\nabla v\|_{L^2(K)^d})^{1/2}, \end{aligned}$$

where

$$\tilde{\eta}_{\Gamma,2,K} = \frac{1}{2} \sum_{\sigma \in \mathcal{F}_K \cap \mathcal{F}_{k,i}} h_K^{-1/2} C_{t,K,\sigma}^{1/2} \|\llbracket \mathbf{t}_k \rrbracket \cdot \mathbf{n}_{\sigma}\|_{L^2(\sigma)}.$$

Setting $\tilde{\eta}_{\Gamma,2}^2 = \sum_{K \in \mathcal{M}_k} \tilde{\eta}_{\Gamma,2,K}^2$, it yields

$$\begin{aligned} \left| \sum_{\gamma \in \Gamma_k} \int_{\gamma} \llbracket \mathbf{t}_k \rrbracket \cdot \mathbf{n}_{\gamma} v \, d\mathbf{y} \right| &\leq \tilde{\eta}_{\Gamma,2} \left(\sum_{K \in \mathcal{M}_k} \|v\|_{L^2(K)}^2 + h_K \|v\|_{L^2(K)} \|\nabla v\|_{L^2(K)^d} \right)^{1/2} \\ &\leq \tilde{\eta}_{\Gamma,2} \left(\|v\|_{L^2(\Omega)}^2 + h_{\mathcal{M}_k} \|v\|_{L^2(\Omega)} \|\nabla v\|_{L^2(\Omega)^d} \right)^{1/2}. \end{aligned}$$

Using the Poincaré inequality $\|v\|_{L^2(\Omega)} \leq d_{\Omega} \|\nabla v\|_{L^2(\Omega)^d}$, where d_{Ω} is the diameter of Ω , we get

$$\left| \sum_{\gamma \in \Gamma_k} \int_{\gamma} \llbracket \mathbf{t}_k \rrbracket \cdot \mathbf{n}_{\gamma} v \, d\mathbf{y} \right| \leq \tilde{\eta}_{\Gamma,2} \left(d_{\Omega}^2 + h_{\mathcal{M}_k} d_{\Omega} \right)^{1/2} \|\nabla v\|_{L^2(\Omega)^d} \leq \tilde{\eta}_{\Gamma,2} c_A^{-1/2} \left(d_{\Omega}^2 + h_{\mathcal{M}_k} d_{\Omega} \right)^{1/2} \|v\|,$$

where c_A is the minimal eigenvalue of $A(\mathbf{x})$ over Ω . The same procedure can be used to replace (4.13e) by a relation avoiding the term $c_{\beta,\mu,K}^{-1/2}$. The new bounds can be used to modify the results of Theorems 3.1 and 3.2 and obtain error estimators when $\mu - \frac{1}{2} \nabla \cdot \beta > 0$ is not satisfied.

5 Numerical Experiments

In order to study the properties and illustrate the performance of the local scheme we consider here several numerical examples. First, we look at the convergence rates of the error estimators, focusing on the errors introduced by solving only local problems. Second, we compute the effectivity indexes of the error estimators and investigate the efficiency of the new local algorithm. To do so, we compare the local scheme against a classical adaptive method, where after each mesh refinement the problem is solved again on the whole domain. The classical method we refer to is given by Algorithm 2.

In all the experiments we use \mathbb{P}_1 elements ($\ell = 1$ in (2.3)) on a simplicial mesh with penalization parameter $\eta_{\sigma} = 10$, the diffusive and convective fluxes $\mathbf{t}_k, \mathbf{q}_k$ are computed with $\varkappa = 0$ (see (4.1)). Furthermore, β is always such that $\nabla \cdot \beta = 0$. These choices give $\eta_{C,1,K} = \eta_{C,2,K} = \tilde{\eta}_{C,1,K} = 0$. For an estimator $\eta_{*,K}$ we define $\eta_*^2 = \sum_{K \in \mathcal{M}_k} \eta_{*,K}^2$. Similarly to [16], if $A = \varepsilon I_2$ and β is constant then

Algorithm 2 ClassicalScheme(\mathfrak{T}_1)

Find $\bar{u}_1 \in V(\mathfrak{T}_1)$ solution to $\mathcal{B}(\bar{u}_1, v_1, \mathfrak{T}_1, 0) = (f, v_1)_1$ for all $v_1 \in V(\mathfrak{T}_1)$.

for $k = 2, \dots, M$ **do**

$(\mathfrak{T}_k, \widehat{\mathfrak{T}}_k) = \text{LocalDomain}(\bar{u}_{k-1}, \mathfrak{T}_{k-1})$.

 Find $\bar{u}_k \in V(\mathfrak{T}_k)$ solution to $\mathcal{B}(\bar{u}_k, v_k, \mathfrak{T}_k, 0) = (f, v_k)_1$ for all $v_k \in V(\mathfrak{T}_k)$.

end for

for $v_k \in H^1(\mathcal{M}_k)$ the augmented norm is well estimated by

$$\begin{aligned} \|v_k\|_{\oplus} \leq \|v_k\|_{\oplus'} &= \|v_k\| + \varepsilon^{-1/2} \|\beta\|_2 \|v_k\|_{L^2(\Omega)} \\ &+ \frac{1}{2} \left(\sum_{K \in \mathcal{M}_k} \left(\sum_{\sigma \in \mathcal{F}_K \cap \mathcal{F}_{k,i}} \tilde{m}_K^{1/2} C_{t,K,\sigma}^{1/2} \|[v_k]\beta \cdot \mathbf{n}_\sigma\|_{L^2(\sigma)} \right)^2 \right)^{1/2}. \end{aligned}$$

Hence, in the numerical experiments we consider the computable norm $\|\cdot\|_{\oplus'}$. The effectivity indexes of the error estimators η and $\tilde{\eta}$ from Theorems 3.1 and 3.2 are defined as

$$\frac{\eta}{\|u - u_k\|} \quad \text{and} \quad \frac{\tilde{\eta}}{\|u - u_k\|_{\oplus'}}, \quad (5.1)$$

respectively. For the solution \bar{u}_k of the classical algorithm we use the error estimators η and $\tilde{\eta}$ from [16]. They are equivalent to the estimators presented in this paper except that for \bar{u}_k we have $\eta_{\Gamma,1,K} = \eta_{\Gamma,2,K} = 0$, as in this case the reconstructed fluxes are in $H_{\text{div}}(\Omega)$. The effectivity indexes for \bar{u}_k are as in (5.1) but with u_k replaced by \bar{u}_k . The numerical experiments have been performed with the help of the C++ library `libMesh` [21].

5.1 Error estimators rate of convergence

In this first example, taken from [16], we solve (1.1) in $\Omega = [0, 1] \times [0, 1]$ with $A = \varepsilon I_2$, $\beta = (1, 0)^\top$ and $\mu = 1$. The force term f is chosen so that the exact solution reads

$$u(\mathbf{x}) = \frac{1}{2} x_1 (x_1 - 1) x_2 (x_2 - 1) (1 - \tanh(10 - 20x_1)), \quad (5.2)$$

see Figure 3(a). The purpose of the current experiment is to investigate the convergence rate of the error estimators for different values of $\varepsilon \in \{1, 10^{-2}, 10^{-4}\}$, i.e. for problems ranging from diffusion to advection dominated. Furthermore, we intentionally want large errors at the subdomains interfaces in order to capture the convergence order of the error estimators $\eta_{\Gamma,1}, \eta_{\Gamma,2}$, hence the local domains are fixed a priori. We define three domains $\Omega_1, \Omega_2, \Omega_3$ as follows: $\Omega_1 = \Omega$, $\mathbf{x} \in \Omega_2$ if $x_1 \in [0.25, 1]$ and $\mathbf{x} \in \Omega_3$ if $x_1 \in [0.375, 0.75]$, see Figure 3(b).

Let h be the grid size of $\widehat{\mathcal{M}}_1$, then the grid sizes of $\widehat{\mathcal{M}}_2$ and $\widehat{\mathcal{M}}_3$ are $h/2$ and $h/4$, respectively. For different choices of h we run Algorithm 1 without calling `LocalDomain`, since the local domains and meshes are chosen beforehand. After the third iteration we compute the exact energy error and the error estimators. The results are reported in Tables 1 to 3 for $\varepsilon = 1$, $\varepsilon = 10^{-2}$ and $\varepsilon = 10^{-4}$, respectively. We recall that η_{NC} measures the non conformity of u_k , η_R measures the error in the energy conservation, η_{DF} the difference between $-A\nabla u_k$ and the reconstructed diffusive flux \mathbf{t}_k , $\eta_U, \eta_{\bar{U}}$ are upwind errors and $\eta_{\Gamma,1}, \eta_{\Gamma,2}$ measure the jumps of $\mathbf{t}_k, \mathbf{q}_k$ across subdomains boundaries.

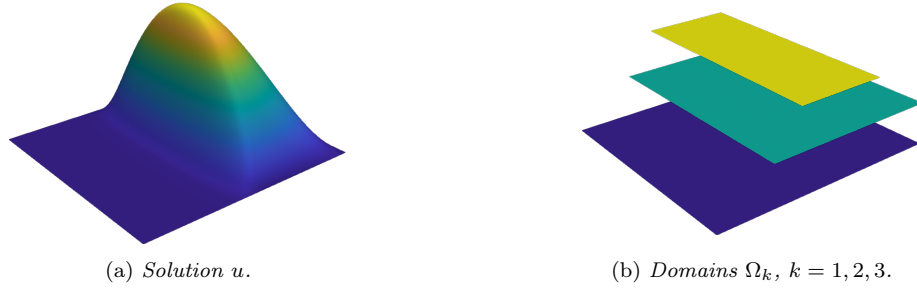


Figure 3. Solution $u(\mathbf{x})$ in (5.2) and local domains.

h	$\ u - u_k\ $	η_{NC}	η_R	η_{DF}	η_U	$\tilde{\eta}_U$	$\eta_{\Gamma,1}$	$\eta_{\Gamma,2}$
2^{-4}	1e-2	2.6e-3	1.9e-3	1.3e-2	3.9e-4	3.6e-4	5.8e-3	3.5e-2
2^{-5}	5e-3	1.3e-3	4.8e-4	6.7e-3	1.3e-4	1.3e-4	4.1e-3	2.4e-2
2^{-6}	2.5e-3	6.3e-4	1.2e-4	3.4e-3	4.6e-5	4.6e-5	2.9e-3	1.7e-2
2^{-7}	1.3e-3	3.1e-4	3e-5	1.7e-3	1.6e-5	1.6e-5	2.1e-3	1.2e-2
Order	1	1	2	1	1.5	1.5	0.5	0.5

Table 1. Section 5.1: convergence rate of error estimators for $\varepsilon = 1$.

h	$\ u - u_k\ $	η_{NC}	η_R	η_{DF}	η_U	$\tilde{\eta}_U$	$\eta_{\Gamma,1}$	$\eta_{\Gamma,2}$
2^{-4}	1e-3	2.7e-4	6.8e-4	1.4e-3	4e-3	3.6e-3	5.8e-3	4.8e-4
2^{-5}	5.1e-4	1.3e-4	1.7e-4	6.8e-4	1.3e-3	1.3e-3	4.1e-3	2.7e-4
2^{-6}	2.5e-4	6.2e-5	4.2e-5	3.4e-4	4.7e-4	4.6e-4	2.9e-3	1.8e-4
2^{-7}	1.3e-4	3.1e-5	1.1e-5	1.7e-4	1.6e-4	1.6e-4	2.1e-3	1.2e-4
Order	1	1	2	1	1.5	1.5	0.5	0.5

Table 2. Section 5.1: convergence rate of error estimators for $\varepsilon = 10^{-2}$.

h	$\ u - u_k\ $	η_{NC}	η_R	η_{DF}	η_U	$\tilde{\eta}_U$	$\eta_{\Gamma,1}$	$\eta_{\Gamma,2}$
2^{-4}	1.1e-4	7.1e-5	6.1e-3	2.5e-4	9.1e-3	7.4e-3	5.9e-3	1.9e-5
2^{-5}	5.2e-5	3.1e-5	1.6e-3	1.2e-4	5.6e-3	5e-3	4.1e-3	9.3e-6
2^{-6}	2.6e-5	1.4e-5	4.1e-4	5.6e-5	3.6e-3	3.5e-3	2.9e-3	5.6e-6
2^{-7}	1.3e-5	5.8e-6	1e-4	2.6e-5	1.7e-3	1.6e-3	2.1e-3	3.5e-6
Order	1	1	2	1	1.5	1.5	0.5	0.5

Table 3. Section 5.1: convergence rate of error estimators for $\varepsilon = 10^{-4}$.

We see that the energy error converges with order one, as predicted by the a priori error analysis of [1]. On the other hand, the error estimators $\eta_{\Gamma,1}$ and $\eta_{\Gamma,2}$ measuring the reconstructed fluxes' jumps across subdomains' boundaries have a rate of convergence of 0.5, of lower order than the other estimators and the true error. Therefore, the error estimators are not efficient, in the sense that they cannot be bounded from above by the energy norm multiplied by a mesh-size independent constant. Hence, the local domains must be chosen so that the jumps at their interfaces are small and thus

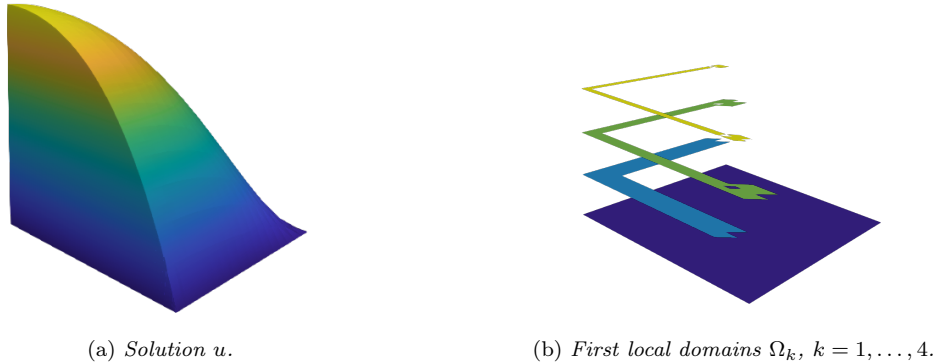


Figure 4. Solution $u(\mathbf{x})$ in (5.3) of the reaction dominated problem and first local domains chosen by the error estimators.

$\eta_{\Gamma,1}$, $\eta_{\Gamma,2}$ are negligible compared to the other estimators; otherwise, the effectivity indexes might be large, in this example they range from 5 to 200. This issue is avoided by taking large enough subdomains covering the large error regions. In the following experiments we let the scheme select the local subdomains on the fly, using the fixed energy fraction marking strategy [13, Section 4.2] implemented in the $\text{LocalDomain}(u_k, \mathfrak{T}_k)$ routine of Algorithm 1.

5.2 Reaction dominated problem

In our next example we consider a symmetric problem and want to compare the local and classical schemes (Algorithms 1 and 2) in a singularly perturbed regime. We investigate the efficiency measured as the computational cost and analyze their effectivity indexes. The setting is as follows: we solve (1.1) in $\Omega = [0, 1] \times [0, 1]$ with $\varepsilon = 10^{-6}$, $A = \varepsilon I_2$, $\boldsymbol{\beta} = (0, 0)^\top$, $\mu = 1$ and we choose f such that the exact solution is given by

$$u(\mathbf{x}) = e^{x_1+x_2} \left(x_1 - \frac{1 - e^{-\zeta x_1}}{1 - e^{-\zeta}} \right) \left(x_2 - \frac{1 - e^{-\zeta x_2}}{1 - e^{-\zeta}} \right), \quad (5.3)$$

where $\zeta = 10^4$. The solution is illustrated in Figure 4(a).

Since the problem is symmetric we have $\|\cdot\| = \|\cdot\|_{\oplus}$, but their related error estimators η and $\tilde{\eta}$, respectively, satisfy $\tilde{\eta} > \eta$ and hence the effectivity index of η will be lower (see Theorems 3.1 and 3.2).

Starting from a coarse mesh (128 elements), we let the two algorithms run for $k = 1, \dots, 20$. In Figure 4(b) we show the first four subdomains Ω_k chosen by the local scheme. The first iterations are needed to capture the boundary layer and reach the convergence regime, hence we will plot the results for $k \geq 7$. The most expensive part of the code is the solution of linear systems by means of the conjugate gradient (CG) method preconditioned with the incomplete Cholesky factorization, followed by the computation of the potential and fluxes reconstruction and then by the evaluation of the error estimators. In the local scheme, the time spent doing these tasks is proportional to the number of elements inside each subdomain Ω_k . For the classical scheme, the cost of these tasks depends on the total number of elements in the mesh. Since the CG routine is the most expensive part, we take the time spent in it as an indicator for the computational cost.

In Figure 5(a), we plot the simulation cost against the error estimator η , for both the local and classical algorithms. Each circle or star in the figure represents an iteration k . We observe that the local scheme provides similar error bounds but at a smaller cost. The effectivity index of η at each iteration k is shown in Figure 5(b), we can observe that the local scheme has an effectivity index similar to the classical scheme.

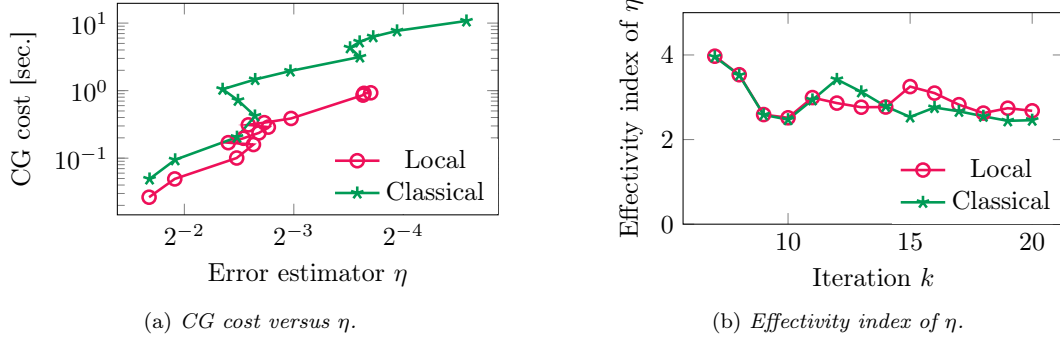


Figure 5. Section 5.2, reaction dominated problem. Computational cost vs. η and effectivity index in function of the iteration number.

In Figure 6(a) we exhibit the cost against the exact energy error and we notice that for some values of k the mesh is refined but the error stays almost constant. This phenomenon significantly increases the simulation cost of the classical scheme without improving the solution. In contrast, the cost of the local scheme increases only marginally. Dividing the two curves in Figure 6(a) we obtain the relative speed-up, which is plotted in Figure 6(b). We note that as the error decreases the local scheme becomes faster than the classical scheme. In Figure 7(a) we plot the effectivity

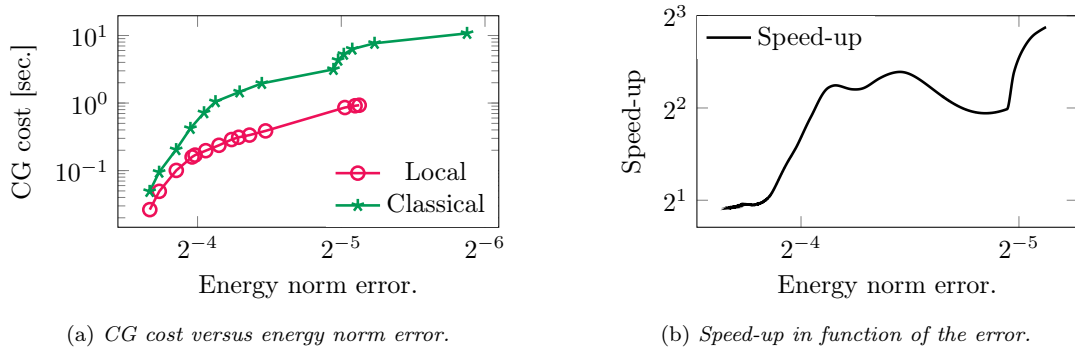
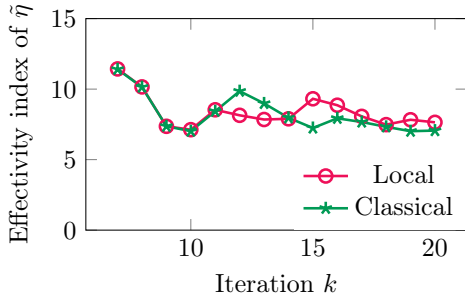
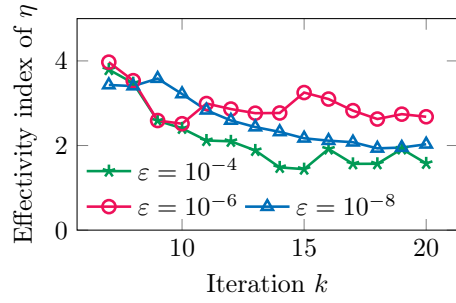


Figure 6. Section 5.2, reaction dominated problem. Computational cost vs. energy norm error and speed-up in function of the error.

index of $\tilde{\eta}$. As expected, for this symmetric problem, it is worse than the effectivity of η . Finally, we run the same experiment but for different diffusion coefficients $\varepsilon = 10^{-4}, 10^{-6}, 10^{-8}$ and display in Figure 7(b) the effectivity index of η . We note that it always remains below 4.



(a) Effectivity index of $\tilde{\eta}$.



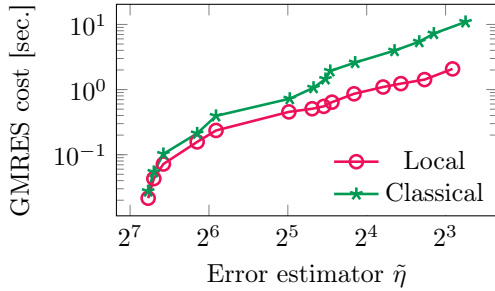
(b) Effectivity index of η for different diffusion coefficients ϵ .

Figure 7. Section 5.2, reaction dominated problem. Effectivity index of $\tilde{\eta}$ and of η but for different diffusion coefficients ϵ .

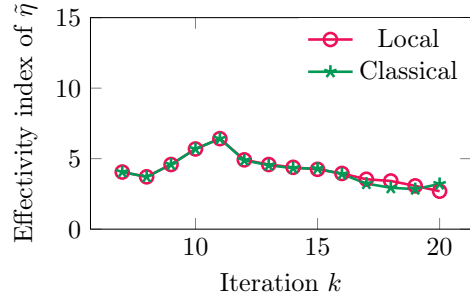
5.3 Convection dominated problem

In this section we perform the same experiment as in Section 5.2 but instead of choosing $\beta = (0, 0)^\top$ we set $\beta = -(1, 1)^\top$, hence we solve a nonsymmetric singularly perturbed problem. The linear systems are solved with the GMRES method preconditioned with the incomplete LU factorization. As in Section 5.2, we investigate the effectivity indexes and efficiency of the local and classical schemes.

For convection dominated problems, the norm $\|\cdot\|_{\oplus}$ is more appropriate than $\|\cdot\|$ since it measures also the error in the advective direction. In Figure 8(a), we plot the simulation cost versus the error estimator $\tilde{\eta}$, we remark that again the local scheme provides similar error bounds at smaller cost. The effectivity index of $\tilde{\eta}$ is displayed in Figure 8(b), we note that the local and classical schemes have again similar effectivity indexes.



(a) GMRES cost versus $\tilde{\eta}$.

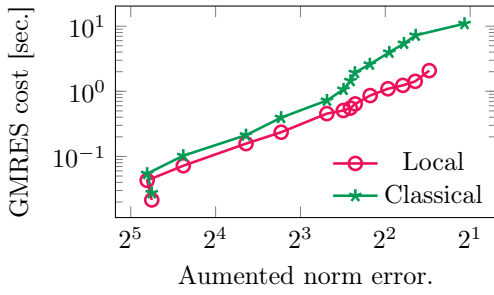


(b) Effectivity index of $\tilde{\eta}$.

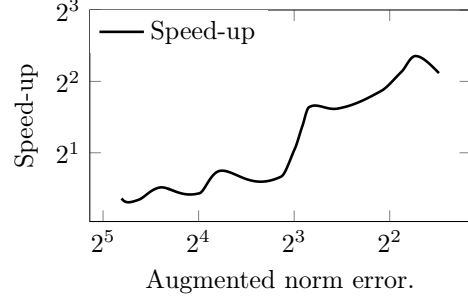
Figure 8. Section 5.3, convection dominated problem. Computational cost vs. $\tilde{\eta}$ and effectivity index in function of the iteration number.

In Figure 9 we plot the simulation cost versus the error in the augmented norm $\|\cdot\|_{\oplus}$ and the relative speed-up. We again observe that the local scheme is faster.

For completeness, we plot in Figure 10(a) the effectivity index of η . We see that it is completely off. This illustrates that this estimator does not capture the convective error and is hence not



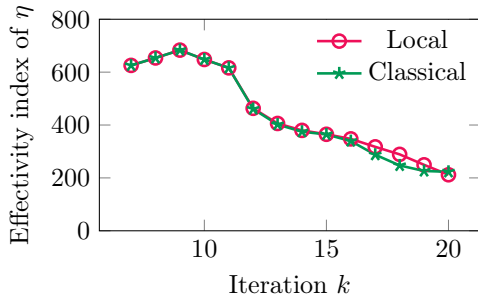
(a) GMRES cost versus augmented norm error.



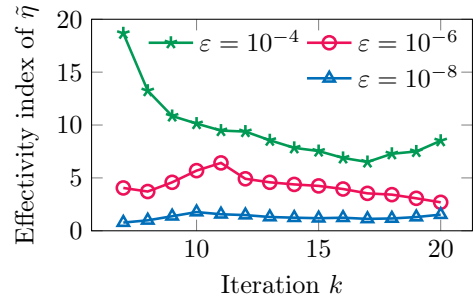
(b) Speed-up in function of the error.

Figure 9. Section 5.3, convection dominated problem. Computational cost vs. augmented norm error and speed-up in function of the error.

appropriate for convection dominated problems. Then, we run again the same experiment but considering different diffusion coefficients $\varepsilon = 10^{-4}, 10^{-6}, 10^{-8}$ and display the effectivity indexes of $\tilde{\eta}$ in Figure 10(b).



(a) Effectivity index of η .



(b) Effectivity index of $\tilde{\eta}$ for different diffusion coefficients ε .

Figure 10. Section 5.3, convection dominated problem. Effectivity index of η and of $\tilde{\eta}$ but for different diffusion coefficients ε .

5.4 A smooth problem

In our last example, we want to apply the local scheme to a smooth problem. We solve (1.1) with $\Omega = [0, 1] \times [0, 1]$, $A = I_2$, $\beta = -(1, 1)^\top$ and $\mu = 1$. The forcing term f is chosen such that the exact solution is given by

$$u(\mathbf{x}) = e^{-\kappa \|\mathbf{x}\|_2} \left(x_1 - \frac{1 - e^{-\kappa x_1}}{1 - e^{-\kappa}} \right) \left(x_2 - \frac{1 - e^{-\kappa x_2}}{1 - e^{-\kappa}} \right) \quad (5.4)$$

with $\kappa = 10$. An illustration of the exact solution is given in Figure 11(a). We run the local and classical schemes for $k = 1, \dots, 15$ starting with a uniform mesh of 128 elements. The first four subdomains chosen by the local scheme are shown in Figure 11(b). For this problem, the

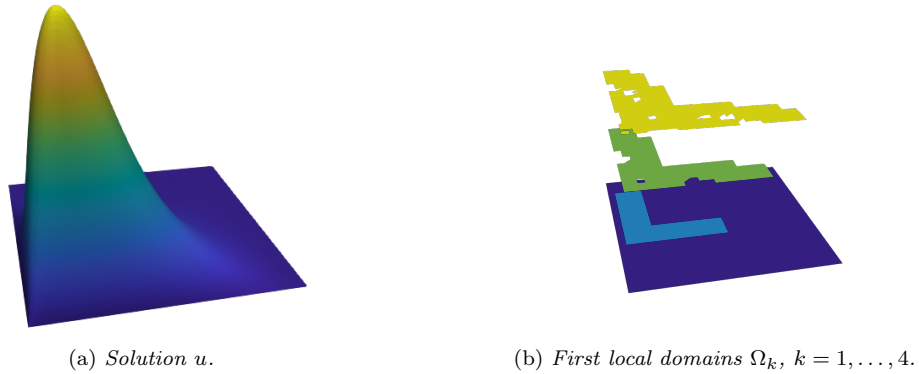


Figure 11. Solution $u(\mathbf{x})$ in (5.4) and first local domains chosen by the error estimators.

error estimators $\eta_{\Gamma,1}$, $\eta_{\Gamma,2}$ measuring the reconstructed fluxes' jumps dominate the other estimators and the effectivity index of the local scheme is larger than the index for the classical scheme, as we illustrate in Figure 12. However, the error estimators of the local scheme are still efficient in

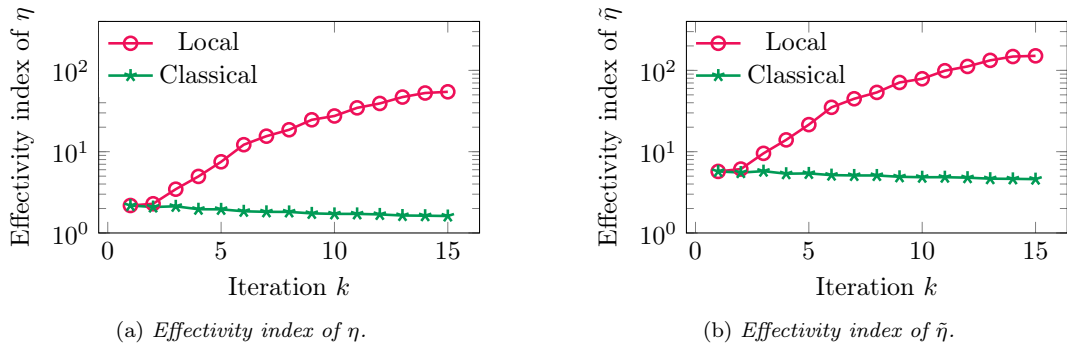


Figure 12. Section 5.4, smooth problem. Effectivity indexes in function of the iteration number.

choosing the appropriate regions to be refined. In Figure 13(a) we show the computational cost in function of the energy errors. We observe that the local method achieves a similar accuracy at a smaller cost. In Figure 13(b) we highlight the relative speed-up of the local scheme and observe that it gets faster as the error decreases. We deduce that the local scheme can be employed also for smooth problems and if a tight estimation of the errors is needed then a full solve at the end of the iteration can be performed.

6 Conclusion

We provide a posteriori error estimators for a local adaptive discontinuous Galerkin method. The scheme, defined in Section 2.2, relies on a coarse solution which is successively improved by solving a sequence of localized elliptic problems in confined subdomains, where the mesh is refined. Starting from error estimators for the symmetric weighted interior penalty Galerkin scheme based on conform-

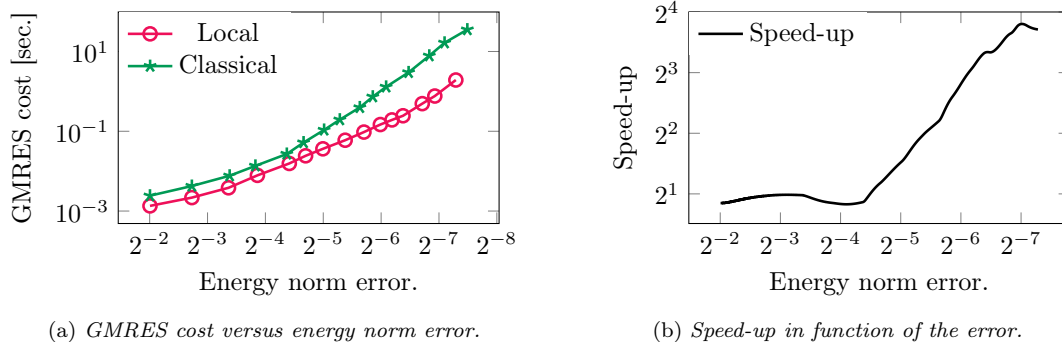


Figure 13. Section 5.4, smooth problem. Computational cost vs. error and speed-up in function of the error.

ing potential and fluxes reconstructions, we allow for flux jumps across the subdomains boundaries and derive new estimators for the local method in Theorems 3.1 and 3.2. An important property of the original estimators (for non local schemes) is conserved: the absence of unknown constants. Numerical experiments confirm the error estimators' robustness for singularly perturbed convection-reaction dominated problems and illustrate the efficiency of the local scheme when compared to a classical adaptive algorithm, where at each iteration the solution on the whole computational domain must be recomputed.

Acknowledgements

The authors are partially supported by the Swiss National Science Foundation, under grant No. 200020_172710.

References

- [1] A. Abdulle and G. Rosilho de Souza. A local discontinuous Galerkin gradient discretization method for linear and quasilinear elliptic equations. *ESAIM: Mathematical Modelling and Numerical Analysis*, 53(4):1269–1303, 2019.
- [2] M. Ainsworth. A synthesis of a posteriori error estimation techniques for conforming, non-conforming and discontinuous Galerkin finite element methods. In *Recent advances in adaptive computation*, volume 383 of *Contemporary Mathematics*, pages 1–14. Amer. Math. Soc., Providence, RI, 2005.
- [3] M. Ainsworth and J. T. Oden. A unified approach to a posteriori error estimation using element residual methods. *Numerische Mathematik*, 65(1):23–50, 1993.
- [4] D. N. Arnold. An interior penalty finite element method with discontinuous elements. *SIAM Journal on Numerical Analysis*, 19(4):742–760, 1982.
- [5] I. Babuška and W. C. Rheinboldt. A-posteriori error estimates for the finite element method. *International Journal for Numerical Methods in Engineering*, 12(10):1597–1615, 1978.

- [6] I. Babuška and W. C. Rheinboldt. Error estimates for adaptive finite element computations. *SIAM Journal on Numerical Analysis*, 15(4):736–754, 1978.
- [7] R. E. Bank and A. Weiser. Some a posteriori error estimators for elliptic partial differential equations. *Mathematics of Computation*, 44(170):283–301, 1985.
- [8] A. Brandt. Multi-level adaptive solutions to boundary-value problems. *Mathematics of Computation*, 31(138):333–390, 1977.
- [9] F. Brezzi and M. Fortin. *Mixed and hybrid finite element methods*, volume 15 of *Springer Series in Computational Mathematics*. Springer-Verlag, New York, 1991.
- [10] I. Cheddadi, R. Fučík, M. I. Prieto, and M. Vohralík. Guaranteed and robust a posteriori error estimates for singularly perturbed reaction-diffusion problems. *ESAIM: Mathematical Modelling and Numerical Analysis*, 43(5):867–888, 2009.
- [11] S. Cochez-Dhondt and S. Nicaise. Equilibrated error estimators for discontinuous Galerkin methods. *Numerical Methods for Partial Differential Equations*, 24(5):1236–1252, 2008.
- [12] D. A. Di Pietro and A. Ern. *Mathematical aspects of discontinuous Galerkin methods*, volume 69 of *Mathématiques et Applications*. Springer, Berlin and Heidelberg, 2012.
- [13] W. Dörfler. A convergent adaptive algorithm for Poisson’s equation. *SIAM Journal on Numerical Analysis*, 33(3):1106–1124, 1996.
- [14] A. Ern, S. Nicaise, and M. Vohralík. An accurate H(div) flux reconstruction for discontinuous Galerkin approximations of elliptic problems. *Comptes Rendus Mathématique*, 345(12):709–712, 2007.
- [15] A. Ern and A. F. Stephansen. A posteriori energy-norm error estimates for advection-diffusion equations approximated by weighted interior penalty methods. *Journal of Computational Mathematics*, 26(4):488–510, 2008.
- [16] A. Ern, A. F. Stephansen, and M. Vohralík. Guaranteed and robust discontinuous Galerkin a posteriori error estimates for convection-diffusion-reaction problems. *Journal of Computational and Applied Mathematics*, 234(1):114–130, 2010.
- [17] A. Ern, A. F. Stephansen, and P. Zunino. A discontinuous Galerkin method with weighted averages for advection-diffusion equations with locally small and anisotropic diffusivity. *IMA Journal of Numerical Analysis*, 29(2):235–256, 2009.
- [18] W. Hackbusch. Local defect correction method and domain decomposition techniques. In K. Böhmmer and H. Stetter, editors, *Defect Correction Methods*, Computing Supplementa, pages 89–113. Springer, Wien, 1984.
- [19] O. A. Karakashian and F. Pascal. A posteriori error estimates for a discontinuous Galerkin approximation of second-order elliptic problems. *SIAM Journal on Numerical Analysis*, 41(6):2374–2399, 2003.
- [20] K. Y. Kim. A posteriori error estimators for locally conservative methods of nonlinear elliptic problems. *Applied Numerical Mathematics*, 57(9):1065–1080, 2007.

- [21] B. S. Kirk, J. W. Peterson, R. H. Stogner, and G. F. Carey. libMesh : a C++ library for parallel adaptive mesh refinement/coarsening simulations. *Engineering with Computers*, 22(3-4):237–254, 2006.
- [22] S. McCormick and J. Thomas. The Fast Adaptive Composite grid (FAC) method for elliptic equations. *Mathematics of Computation*, 46(174):439–456, 1986.
- [23] J. Nédélec. Mixed finite elements in \mathbb{R}^3 . *Numerische Mathematik*, 35(3):315–341, 1980.
- [24] L. Payne and H. Weinberger. An optimal Poincaré inequality for convex domains. *Archive for Rational Mechanics and Analysis*, 5(1):286–292, 1960.
- [25] P. Raviart and J. Thomas. A mixed finite element method for 2nd order elliptic problems. In E. Magenes and I. Galligani, editors, *Mathematical aspects of finite element methods (Proc. Conf., Consiglio Naz. delle Ricerche (C.N.R.), Rome, 1975)*, volume 606 of *Lecture Notes in Mathematics*, pages 292–315, New York, 1977. Springer-Verlag.
- [26] G. Rosilho De Souza. *Numerical methods for deterministic and stochastic differential equations with multiple scales and high contrasts*. PhD thesis, EPFL, 2020.
- [27] A. F. Stephansen. *Méthodes de Galerkin discontinues et analyse d’erreur a posteriori pour les problèmes de diffusion hétérogène*. PhD thesis, Ecole Nationale des Ponts et Chaussées, 2007.
- [28] R. Verfürth. *A review of a posteriori error estimation and adaptive mesh-refinement techniques*. Wiley-Teubner, New York, 1996.
- [29] M. Vohralík. Residual flux-based a posteriori error estimates for finite volume and related locally conservative methods. *Numerische Mathematik*, 111(1):121–158, 2008.